Neurobiology of Disease

Conditional Deletion of *Prnp* Rescues Behavioral and Synaptic Deficits after Disease Onset in Transgenic Alzheimer's Disease

Santiago V. Salazar,[1,2] Christopher Gallardo,[3] Adam C. Kaufman,[1] Charlotte S. Herber,[1] Laura T. Haas,[1,4] Sophie Robinson,[1] Jean C. Manson,[5] Michael K. Lee,[3] and Stephen M. Strittmatter[1]

[1]Cellular Neuroscience, Neurodegeneration, Repair, Department of Neurology and of Neuroscience, Yale University School of Medicine, New Haven, Connecticut 06536, [2]Department of Genetics, Yale University School of Medicine, New Haven, Connecticut 06520, [3]Department of Pharmacology, and Department of Neuroscience, Institute for Translational Neuroscience, University of Minnesota, Minneapolis, Minnesota 55455, [4]Graduate School of Cellular and Molecular Neuroscience, University of Tuebingen, D-72074 Tuebingen, Germany, and [5]The Roslin Institute, University of Edinburgh, Midlothian, EH25 9RG, United Kingdom

Biochemical and genetic evidence implicate soluble oligomeric amyloid-β (Aβo) in triggering Alzheimer's disease (AD) pathophysiology. Moreover, constitutive deletion of the Aβo-binding cellular prion protein (PrP^C) prevents development of memory deficits in APP_{swe}/PS1ΔE9 mice, a model of familial AD. Here, we define the role of PrP^C to rescue or halt established AD endophenotypes in a therapeutic disease-modifying time window after symptom onset. Deletion of *Prnp* at either 12 or 16 months of age fully reverses hippocampal synapse loss and completely rescues preexisting behavioral deficits by 17 months. In contrast, but consistent with a neuronal function for Aβo/PrP^C signaling, plaque density, microgliosis, and astrocytosis are not altered. Degeneration of catecholaminergic neurons remains unchanged by PrP^C reduction after disease onset. These results define the potential of targeting PrP^C as a disease-modifying therapy for certain AD-related phenotypes after disease onset.

Key words: Alzheimer's; memory; prion; transgenic

Significance Statement

The study presented here further elucidates our understanding of the soluble oligomeric amyloid-β–Aβo-binding cellular prion protein (PrP^C) signaling pathway in a familial form of Alzheimer's disease (AD) by implicating PrP^C as a potential therapeutic target for AD. In particular, genetic deletion of *Prnp* rescued several familial AD (FAD)-associated phenotypes after disease onset in a mouse model of FAD. This study underscores the therapeutic potential of PrP^C deletion given that patients already present symptoms at the time of diagnosis.

Introduction

Alzheimer's disease (AD) is the most common form of dementia worldwide, affecting >5 million Americans (Alzheimer's Association, 2012). AD is characterized by two hallmark pathologies: amyloid-β (Aβ) plaques composed of Aβ peptide and neurofibrillary tangles composed of hyperphosphorylated Tau (Braak and Braak, 1991; Selkoe, 2011). The clinical presentation of AD is characterized by progressive memory loss and early death (Mölsä et al., 1986; Mayeux, 2003). Central to AD is the inability of patients to form new memories, with synaptic dysfunction and loss being tightly correlated with symptom progression (Selkoe, 2002; Scheff et al., 2006). Therefore, understanding how synapses are lost is key to understanding AD. Genetic and biochemical evidence suggest a soluble high-molecular weight oligomeric amyloid-β peptide (Aβo) as a trigger for synaptic dysfunction in AD (Hardy and Selkoe, 2002; Sheng et al., 2012; Dohler et al., 2014; Kostylev et al., 2015). Several studies in rodent models have shown that Aβo can initiate a cascade of deleterious effects on

Received March 16, 2017; revised July 17, 2017; accepted Aug. 11, 2017.

Author contributions: S.V.S., C.G., A.C.K., L.T.H., M.K.L., and S.M.S. designed research; S.V.S., C.G., A.C.K., C.S.H., L.T.H., and S.R. performed research; J.C.M. contributed unpublished reagents/analytic tools; S.V.S., C.G., A.C.K., C.S.H., L.T.H., and S.M.S. analyzed data; S.V.S., M.K.L., and S.M.S. wrote the paper.

This work was supported by the National Institutes of Health, the BrightFocus Foundation, the Alzheimer's Association, and Falk Medical Research Trust (all to S.M.S.). We thank Stefano Sodi for assistance with mouse husbandry and Jillian Friedrich for technical assistance with sectioning the brains.

S.M.S. is a cofounder of Axerion Therapeutics seeking to develop PrP^C-based therapeutics for Alzheimer's disease. The remaining authors declare no competing financial interests.

Correspondence should be addressed to Stephen M. Strittmatter, CNNR Program, BCMM 436, Yale University School of Medicine, 295 Congress Avenue, New Haven, CT 06536. E-mail: Stephen.Strittmatter@yale.edu.

DOI:10.1523/JNEUROSCI.0722-17.2017

 0270-6474/17/379207-15$15.00/0

synaptic function (Lambert et al., 1998; Walsh et al., 2002; Lesné et al., 2006; Shankar et al., 2008). These studies highlight the importance of understanding Aβo-dependent synaptotoxicity.

Recent evidence suggests Aβo-binding cellular prion protein (PrP^C) as a central protein in mediating synaptotoxicity. Previous work has shown PrP^C as a high-affinity binding partner of Aβo and a mediator in suppressing LTP (Laurén et al., 2009). In addition, constitutive deletion of *Prnp* can rescue synapse density, survival, and learning and memory deficits seen in a mouse model of familial AD (Gimbel et al., 2010). Other groups have shown PrP^C to bind Aβo with high affinity (Chen et al., 2010; Dohler et al., 2014), mediate suppression of LTP (Barry et al., 2011; Freir et al., 2011; Klyubin et al., 2014), and suppress learning and memory (Chung et al., 2010; Fluharty et al., 2013). Nevertheless, conflicting reports of the role for PrP^C in mediating synaptotoxicity (Balducci et al., 2010; Calella et al., 2010; Kessels et al., 2010) have prompted further studies to test the therapeutic potential of PrP^C as a target.

Targeting PrP^C for AD treatment holds the potential for disease-modifying therapy, as opposed to the symptomatic action of current interventions approved for AD (Yiannopoulou and Papageorgiou, 2013). Several studies have shown directly or indirectly that Aβo binding to PrP^C leads to PrP^C-mGluR5 coupling (Um et al., 2013; Haas et al., 2016) and subsequent activation of intracellular components including eEF2 (Um et al., 2013; Ma et al., 2014) and Fyn (Larson et al., 2012; Um et al., 2012; Rushworth et al., 2013; Kaufman et al., 2015) can lead to dendritic spine loss (Um et al., 2012; Zhang et al., 2015), suppressed synaptic plasticity (Hu et al., 2014; Haas et al., 2016), and Tau phosphorylation (Larson et al., 2012; Kaufman et al., 2015). Multiple groups have begun to develop methods to target the Aβo-PrP^C interaction using small-molecule approaches (Fluharty et al., 2013; Aimi et al., 2015; Osborne et al., 2016) and immunotherapy approaches (Chung et al., 2010; Barry et al., 2011). These efforts underscore the need to understand whether the Aβo-PrP^C interaction is required for AD phenotype maintenance and progression after disease onset.

To test the therapeutic potential of targeting *Prnp*, we decided to take advantage of a tamoxifen (TMX)-inducible Cre-lox system to partially delete *Prnp* early after disease onset and months after disease onset in a mouse model of familial AD. Partial deletion of *Prnp* was able to rescue synaptic and behavioral deficits in a mouse model of AD at 12 and 16 months. These results highlight the clinical potential of targeting the Aβo–PrP^C interaction.

Materials and Methods

Animals

All mice were cared for by the Yale Animal Resource Center. Yale's institutional animal care and use committee approved all experiments. As described previously (Gimbel et al., 2010), the mouse strains used were the APP_{swe}/PSEN1ΔE9 mice on a C57BL/6J background and ER-Cre mice (Hayashi and McMahon, 2002) on a C57BL/6J background were purchased from The Jackson Laboratory. Flox-*Prnp* mice on a C57BL6 background have been described previously (Tuzi et al., 2004; Bradford et al., 2009). All experiments used littermate control mice. The group receiving *Prnp* deletion at 12 months (hereafter referred to as the 12MD cohort) contained a 2:1 male to female sex ratio and the group receiving *Prnp* deletion at 16 months (hereafter referred to as the 16MD cohort) contained a 1.1:1 male to female sex ratio. The differential male to female sex ratios were not intentional, but rather were caused by random breeding and selection.

Brain tissue collection

Immunohistology. Mice were killed and immediately perfused with ice-cold phosphate buffer saline (PBS) for 2 min, followed by a five-minute perfusion with ice-cold 4% paraformaldehyde (PFA). Brains were dissected out, cut down the midline into two hemispheres and fixed for 24 h in 4% PFA. Following fixation, brains were cut into 40 μm parasagittal sections using a Leica (Wetzlar, Germany) WT1000S Vibratome. Sections were stored in PBS at 4°C until staining.

Biochemistry. Mice were killed as above and brains were dissected out immediately. Cortex, hippocampus, and cerebellum were dissected out separately and from each hemisphere. The left hemisphere was flash frozen in liquid nitrogen and the right hemisphere was homogenized in a volume three times the brain weight with TBS containing PhosSTOP and cOmplete-mini to extract the cytosolic fraction. Homogenate was centrifuged at 100,000 × *g* for 20 min at 4°C. The supernatant was collected as TBS soluble and the pellet was resuspended in equal volume as the TBS volume of RIPA buffer containing PhosSTOP and cOmplete-mini. This homogenate was centrifuged at 100,000 × *g* at 4°C for 20 min and the supernatant was collected as the RIPA-soluble extract. The pellet was flash frozen in liquid nitrogen and stored at −80°C. Protein concentrations of the TBS- and RIPA-soluble fractions were quantified using a BCA assay (Thermo Scientific).

Immunohistology

Free-floating 40 μm sections were washed in a 12-well plate once with 0.1% PBS–Triton X-100 for 5 min. Subsequently, sections were blocked with 5% normal horse serum (NHS) in PBS for 1 h at room temperature. Sections were then incubated in primary antibody with 5% NHS in PBS overnight at 4°C. The following primary antibodies were used: mouse anti-PrP^C (8H4) (Abcam, #ab61409, 1:1000), rabbit anti-β-Amyloid (Cell Signaling Technology, #2454, 1:250), rabbit anti-PSD-95 (Invitrogen, #51-6900, 1:250), rabbit anti-SV2A (Abcam, #ab32942, 1:250), chicken anti-GFAP (Abcam, #ab4674, 1:500), and rabbit anti-Iba1 (Wako Chemicals, #019-19741, 1:250). Sections were washed five times after primary incubation with PBS for 10 min each. Sections were then incubated with fluorescent secondary antibodies (donkey anti-rabbit or donkey anti-chicken; Invitrogen, Alexa Fluor, 1:500) for 1 h at room temperature. Samples were washed three times in PBS. To quench lipofuscin autofluoresence for PrP^C staining, samples were incubated in 10 mM $CuSO_4$ in ammonium acetate for 15 min (Schnell et al., 1999) after secondary antibody. The samples were washed one with PBS and mounted onto glass slides (Superfrost Plus; Thermo Scientific) and mounted using Vectashield (Vector Laboratories).

Immunoblots and ELISA/PLISA

All samples were run on a precast 4–20% Tris-glycine gel (Bio-Rad Laboratories) and then transferred to a nitrocellulose membrane using iBlot gel transfer stacks (Novex Life Technlogies). After transferring, membranes were washed in blocking buffer (Rockland, #MB-070) for 1 h at room temperature followed by overnight incubation at 4°C with the following antibodies: mouse anti-PrP^C (SAF-32; Cayman, #189720; 1:200), rabbit anti-Doppel (ab23701, 1:500), mouse anti-β-Actin (Cell Signaling Technology, #3700, 1:10,000), rabbit anti-eEF2 (Cell Signaling Technology, #2332; 1:1000), and rabbit anti-phospho-eEF2 (Cell Signaling Technology, #2331; 1:1000). The membranes were then washed 3 times in 0.1% TBS-Tween 20 and incubated with secondary antibody (Odyssey donkey anti-rabbit and donkey anti-mouse conjugated to IRDye 680 or IRDye 800 at 1:20,000) in blocking buffer for 1 h at room temperature. Finally, membranes were washed 3 times in 0.1% TBS-Tween 20 and developed using a LI-COR Infrared Imaging system. Densitometric analysis was performed using Image Studio Lite (LI-COR).

ELISA was used to measure human amyloid-β 40 (Life Technologies, #KHB3481) and human amyloid-β 42 as per the manufacturer's instructions. The TBS-soluble cortical lysate was homogenized with 1:6 (w/v) and diluted in standard diluent buffer at a 1:1 ratio. RIPA-soluble cortical lysates were homogenized as described above and diluted in standard diluent buffer at 1:5. The absorbance at 450 nm was measured using a Victor 3V plate reader (PerkinElmer Life Sciences). The absolute amount of a $Aβ_{40}$ or $Aβ_{42}$ was calculated using the standard curve based on serial dilutions of monomeric synthetic $Aβ_{40}$ or $Aβ_{42}$ and normalized to original tissue weight. A modified ELISA was used to measure PrP^C-interacting Aβo as described previously (Um et al., 2012). Briefly, a plate-based assay was used

for measuring PrP^C-interacting Aβo to achieve higher sensitivity. Low-volume high-binding white microplates (Greiner, #784074) were coated overnight with 20 μl/well of 250 nM human PrP^C AA23-111 in 30 mM Na_2CO_3, 80 mM $NaHCO_3$, pH 9.6, at 4°C. After washing twice with PBST (PBS, 0.05% Tween 20), the plates were blocked with 25 μl/well protein-free T20 PBS blocking buffer (Pierce) for 4 h at room temperature. After washing 3 times with PBST, 20 μl of TBS soluble samples diluted 1:2–1:4 in PBSTB (PBS, 0.05% Tween 20, 0.5% bovine serum albumin) were applied to microplates in triplicate and incubated overnight at 4°C. Two-fold serial dilutions of synthetic Aβo in PBSTB (0–10 nM range) were included in each plate as a standard curve. Plates were then washed four times with PBST and incubated with D54D2 anti-Aβ antibody (epitope in the N terminus of Aβ peptide; Cell Signaling Technology, #8243) diluted 1:2000 in PBSTB for 2 h. After washing four times in PBST to remove the unbound primary antibody, 20 μl/well of 1:8000 dilution of Eu-N1 goat anti-rabbit IgG (PerkinElmer Life Sciences) in DELFIA assay buffer (PerkinElmer Life Sciences) was applied for 1 h. Finally, after washing five times in PBST, 20 μl of DELFIA Enhancement Solution (PerkinElmer Life Sciences) was applied to each well and time-resolved europium fluorescence was measured using a Victor 3V plate reader (PerkinElmer Life Sciences).

Imaging and analysis of immunohistochemistry

An UltraVIEW VoX (PerkinElmer) spinning disc confocal microscope with 60× 1.3 numerical aperture oil-immersion lens was used to analyze PrP^C, PSD-95, and SV2A staining. For PrP^C staining, three images were captured from the stratum radiatum and cortex from each section with two sections per animal to calculate mean fluorescence intensity (MFI) using ImageJ software. For PSD-95 and SV2A staining, two 40 μm hippocampus containing sections were chosen at random. Three images of the mossy fibers in the dentate gyrus were collected for each slice and ImageJ was used to calculate the area occupied by immunoreactive puncta and averaged per mouse. A Zeiss AxioImager ZI fluorescent microscope (4× and 20× air-objective lens) was used to image and analyze β-amyloid, GFAP, and Iba1 staining. The hippocampus of each mouse was imaged and the immunoreactive percentage area was analyzed using ImageJ (n = averaged percentage positive area for one mouse).

Tamoxifen treatment

All mice used in the experiments were treated with tamoxifen after the first round of behavioral experiments. Tamoxifen was solubilized in sunflower oil to 10 mg/ml with heating at 37°C and sonication was repeated. All mice received a 100 mg/kg dose by oral gavage for 3 d and behavior was analyzed 21 d after treatment after the last day of treatment. Mice were treated at 12 or 16 months (see Figure 1).

Degeneration of catecholaminergic neurons

Immunohistology. Forty-micrometer coronal sections were placed serially into 12-well plates with cryoprotectant. Tissue sections were washed with TBS and incubated with a polyclonal anti-tyrosine hydroxylase (TH; Millipore, #AB152, 1:2000) antibody overnight at 4°C. Sections were washed in TBS and incubated in a biotin-conjugated anti-rabbit (Jackson Laboratories) secondary antibody. Sections were visualized with ABC (Vector Laboratories, #PK-6100) and DAB (Sigma-Aldrich, #D4418) was used as the chromogen. Sections were then mounted, counterstained with cresyl violet, and coverslipped after a series of alcohol dehydrations.

Stereological analyses. Stereological sampling was performed using StereoInvestigator software (MicroBrightField) as described previously (Liu et al., 2008). Cell body analyses were conducted with the optical fractionator for counting the number of neurons and the nucleator for neuronal volume analysis of neurons in the locus ceruleus (LC) (Liu et al., 2008). Sampling parameters include a 40 × 30 μm counting frame, a guard height of 2 μm, a 100 × 100 μm sampling grid, and a dissector height of 18 μm. Every fourth section was taken for neuronal analyses, yielding three to five sections for the LC region. The nucleator probes were applied to anteromedial sections of the LC. Gundersen (m = 1) coefficients of error were <0.1.

Behavioral testing

The order of behavioral testing was rotarod, novel object recognition (NOR), Morris water maze (MWM), and passive avoidance test (PAT) last. Exclusion criteria were used for each test as described below. Exclusion criteria for one test were independent of any other test.

Rotarod. The experimenter was blind to genotype status of all animals. The rotarod used for all experimentation was done on an Economex apparatus (Columbus Instruments). Mice were brought to the testing room and allowed to adjust to the new environment for 15 min before testing began. Mice were gently placed on a stationary rod. The mice were oriented in such a way that would allow them to walk forward to maintain balance once the test began. The rod's initial speed was 2 rotations/min with an acceleration of 0.2 rotations/s. Mice were tested on the rotarod 5 times/d for a 3 d period to acclimate them to the task. On the fourth day, the mice were tested on the rotarod six times and their time until falling off the rod was recorded. Each mouse's shortest and longest time on the rod was discarded. The remaining times for each mouse were averaged together to create a single value for each mouse. If a mouse was unable to stay on the rod for longer than 10 s after 3 d of training, that mouse was not tested.

NOR. As described in Zhang et al. (2012), mice were handled for 5 min a day for 5 d before the experiment to reduce anxiety. Mice were habituated to clean, rectangular, empty rat cages in a dimly lit behavioral testing room for 1 h. The cage was centered in front of the experimenter and oriented with the short axis perpendicular to the test administrator. During the acquisition trial, mice were removed from the behavioral cage and 2 identical objects, either a single 15 ml conical tube with orange cap or a wrapped 5 ml plastic syringe, were placed 1 inch from the edge of either end of the long axis of the cage perpendicular to the long axis. Object choice was pseudorandom; the object was recorded as the familiar object for each animal. The mouse was then replaced in cage's center not facing either object and a total timer counted up to 10 min. The mice were allowed to explore the object and the time it took to accumulate 30 s of total orofacial object exploration was recorded. Orofacial is defined as whisking or sniffing. Finally, mice were left for 10 min with the objects in the behavior cage. Then, the objects were removed and discarded and the mice were left in their cages for 1 h.

During the test trial, one of both the novel and familiar objects were placed on pseudorandom sides of the cage. Orofacial exploration of each object was timed until a combined total of 30 s was reached. After the trial and acquisition trial of each mouse, cages were cleaned to eliminate scent cues. The experimenter was blind to object novelty and genotype. Mice that did not explore both objects, had barbered whiskers, or failed to reach 30 s of exploration during either trial <6 min were eliminated.

MWM. Animals were randomly assigned to treatment groups and the experimenter was blind to both genotype and treatment status. Each mouse was handled for 5 min for the 5 d leading up to any behavioral testing to reduce anxiety. MWM testing was completed in 3 d blocks with probe trial performed on the fourth day. Mice were repeatedly placed in an open water pool ~1 m in diameter to find a submerged hidden platform. Clear and colorless water remained at room temperature throughout all aspects of the experiment. The location of the platform remained fixed in the center of one of the quadrants (target quadrant) of the pool throughout the entire testing period. Visual cues remained constant throughout forward and reverse swims. The mice had a total of eight attempts per day to locate the platform and training was divided into two blocks of four. The first block of four attempts was performed in the morning and the second block of four was performed in the afternoon. The order that the mice were tested in remained constant. The mice were gently placed into the pool facing the wall at one of four locations located in the opposite hemisphere from where the platform was and the latency to finding the platform was timed. The order of the four locations used to start the mice varied for each block to ensure that the mice would have to rely on spatial cues to find the platform. Once a mouse spent 1 s on the platform, the attempt was considered complete and the mouse would be removed from the pool. If a mouse did not find the platform within 60 s, it was guided to the platform and allowed to spend 10 s on the platform, after which it was removed from the pool.

Twenty-four hours after the completion of the last block, the mice were tested in a probe trial. The probe trial consisted of returning the mice to the pool to explore for a single trial of 60 s with the hidden

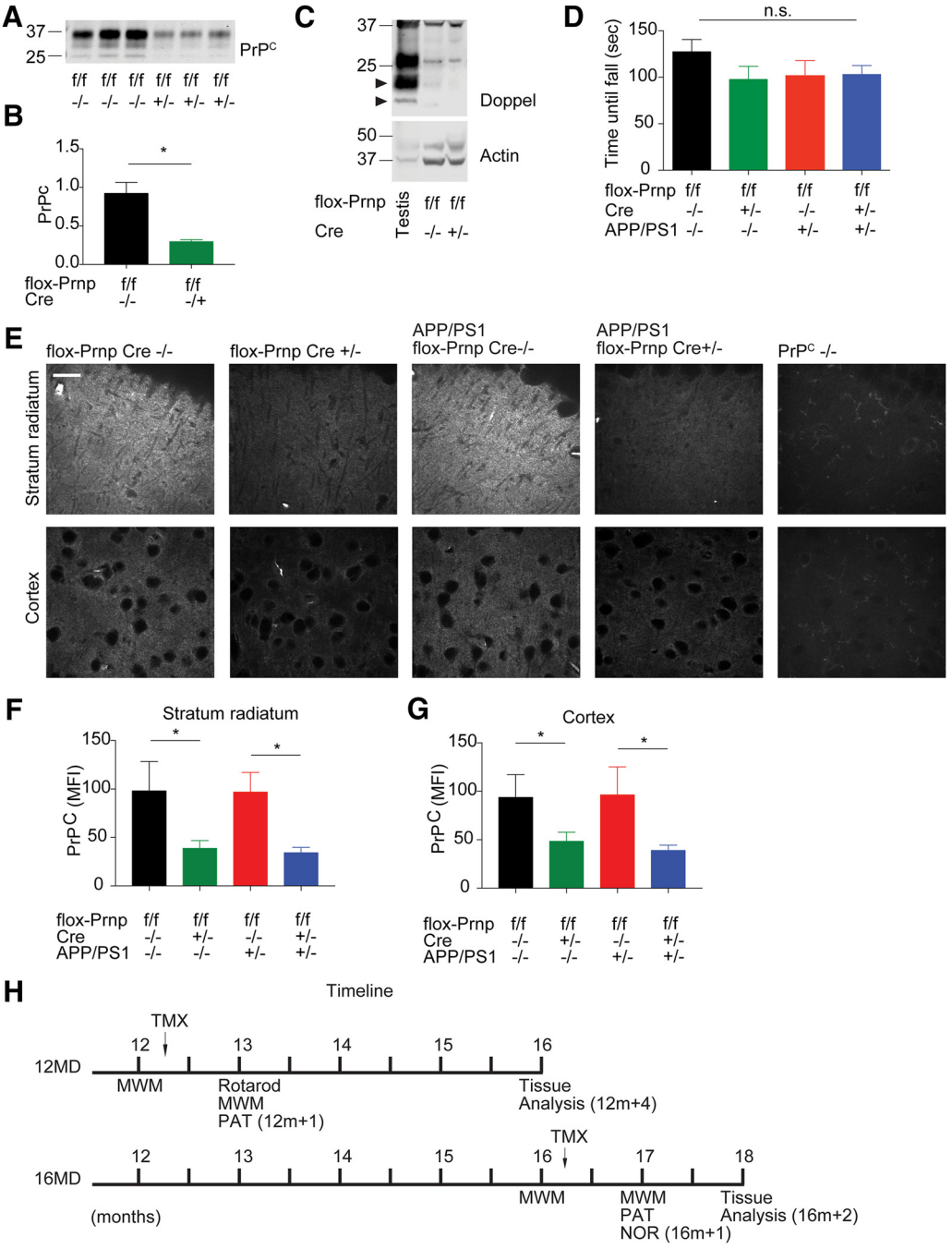

Figure 1. Tamoxifen-inducible Cre-mediated deletion of *Prnp* reduces PrP^C expression and does not activate Doppel expression or induce motor deficits. ***A***, Representative immunoblot of PrP^C after *Prnp* deletion in 12MD cohort using a tamoxifen-inducible Cre system. Each lane represents cortical lysate from one mouse at 12m+4 (***H***). ***B***, Densitometric analysis of immunoblot from ***A*** normalized to total protein levels. Data are graphed as mean ± SEM, $n = 3$ flox-*Prnp* Cre $^{-/-}$ mice, $n = 3$ flox-*Prnp* Cre $^{-/+}$ mice. There was a significant decrease in PrP^C levels after tamoxifen treatment (unpaired two-tailed Student's *t* test, $^*p < 0.05$). ***C***, Representative immunoblot of Doppel expression in 12-month-old mice with and without Cre activation. Arrowhead denotes Doppel band. Testis is used as a positive control. Equal amounts of protein loaded in each lane for all blots. ***D***, Rotarod test was performed on all experimental genotypes in the 12MD cohort at 12m+1 to determine potential motor deficits. There was no significant change between genotypes by one-way ANOVA. Data are graphed as mean ± SEM, $n = 4$ flox-*Prnp* Cre $^{-/-}$ mice, $n = 4$ flox-*Prnp* Cre $^{-/+}$ mice, $n = 5$ APP/PS1 flox-*Prnp* Cre $^{-/-}$ mice, $n = 4$ APP/PS1 flox-*Prnp* Cre $^{-/+}$ mice. ***E***, Representative immunofluorescent images from the stratum radiatum of the hippocampus (top) and cortex (bottom) stained with anti-PrP^C (8H4) antibody from the 12MD cohort at 12m+4. Images were captured using a confocal microscope with a 60× objective. Scale bar, 10 μm. ***F***, ***G***, Quantification of immunoreactive PrP^C MFI for the indicated genotypes in the stratum radiatum (***F***) and cortex (***G***). Two 40 μm slices per animal were analyzed. Data are graphed as mean ± SEM per animal and normalized to flox-*Prnp* Cre $^{-/-}$ mice. For ***F***, $n = 6$ flox-*Prnp* Cre $^{-/-}$ mice, $n = 6$ flox-*Prnp* Cre $^{-/+}$ mice, $n = 5$ APP/PS1 flox-*Prnp* Cre $^{-/-}$ mice, $n = 5$ APP/PS1 flox-*Prnp* Cre $^{-/+}$ mice. For ***G***, $n = 6$ flox-*Prnp* Cre $^{-/-}$ mice, $n = 6$ flox-*Prnp* Cre $^{-/+}$ mice, $n = 6$ APP/PS1 flox-*Prnp* Cre $^{-/-}$ mice, $n = 5$ APP/PS1 flox-*Prnp* Cre $^{-/+}$ mice. flox-*Prnp* mice with Cre have significantly less immunoreactive PrP^C MFI compared with Cre $^{-/-}$ controls (one-way ANOVA with uncorrected Fisher's LSD multiple-comparison test; $^*p < 0.05$). ***H***, Timeline representing the experimental design. Early *Prnp* deletion at 12 months (12MD) is represented by the top timeline and late *Prnp* deletion at 16 months (16MD) is represented by bottom timeline. Black arrow represents tamoxifen injection of all animals regardless of genotype.

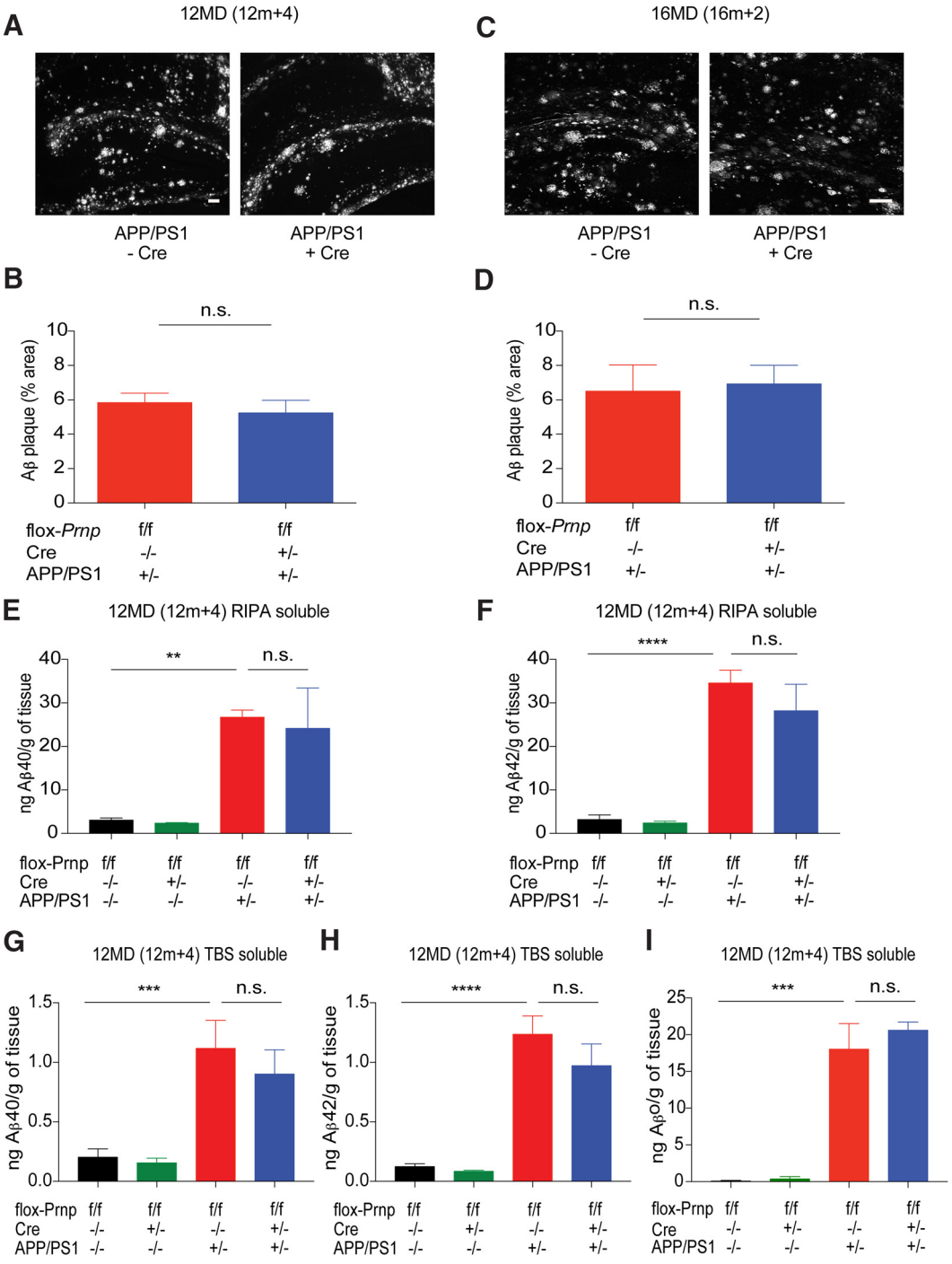

Figure 2. APP metabolism remains unchanged with conditional deletion of *Prnp*. ***A***, Representative immunofluorescent images of the hippocampus stained with anti-Aβ antibody from 12MD cohort at 12m+4. Images were captured using a fluorescent microscope with a 4× objective. Scale bar, 10 μm. ***B***, Quantification of Aβ-immunoreactive percentage area in the hippocampus for indicated genotypes. Two slices per animal were analyzed. There is no statistical difference between genotypes by unpaired two-tailed Student's *t* test. Data are graphed as mean ± SEM per animal, $n = 6$ APP/PS1 flox-*Prnp* Cre $^{-/-}$ mice, $n = 6$ APP/PS1 flox-*Prnp* Cre $^{-/+}$ mice. ***C***, Representative immunofluorescent images of the hippocampus stained with anti-Aβ antibody from the 16MD cohort at 16m+2. Images were captured using a confocal microscope with a 10× objective. Scale bar, 10 μm. ***D***, Quantification of Aβ-immunoreactive percentage area in the hippocampus for indicated genotypes. Two slices per animal were analyzed. There is no statistical significance between genotypes by unpaired *t* test. Data are graphed as mean ± SEM per animal, $n = 6$ APP/PS1 flox-*Prnp* Cre $^{-/-}$ mice, $n = 6$ APP/PS1 flox-*Prnp* Cre $^{-/+}$ mice. ***E***, ***F***, RIPA-soluble cortical lysates from the 12MD cohort at 12m+4 were analyzed for Aβ_{40} (***E***) and Aβ_{42} (***F***) levels by ELISA. There is a significant increase between flox-*Prnp* Cre $^{-/-}$ and APP/PS1 flox-*Prnp* Cre $^{-/-}$ mice, but the presence of Cre had no effect on RIPA-soluble Aβ_{40} or Aβ_{42} levels (one-way ANOVA with uncorrected Fisher's LSD multiple-comparisons test; $^{**}p < 0.01$, $^{****}p < 0.0001$). Data are graphed as mean ± SEM per animal. For ***E*** and ***F***, $n = 6$ flox-*Prnp* Cre $^{-/-}$ mice, $n = 6$ flox-*Prnp* Cre $^{-/+}$ mice, $n = 6$ APP/PS1 flox-*Prnp* Cre $^{-/-}$ mice, $n = 6$ APP/PS1 flox-*Prnp* Cre $^{-/+}$ mice. ***G–I***, TBS-soluble cortical lysates from the 12MD cohort at 12m+4 were analyzed for Aβ_{40} (***G***) and Aβ_{42} (***H***) by ELISA and PrP^{C}-interacting Aβo (***I***) levels were measured by a modified ELISA, PLISA (see Materials and Methods). There is a significant increase between flox-*Prnp* Cre $^{-/-}$ and APP/PS1 flox-*Prnp* Cre $^{-/-}$ mice, but the presence of Cre had no effect on TBS-soluble Aβ_{40}-, Aβ_{42}-, or PrP^{C}-interacting Aβo levels. (one-way ANOVA with uncorrected Fisher's LSD multiple-comparisons test; $^{***}p < 0.001$, $^{****}p < 0.0001$). Data are graphed as mean ± SEM per animal. For ***G*** and ***H***, $n = 6$ flox-*Prnp* Cre $^{-/-}$ mice, $n = 6$ flox-*Prnp* Cre $^{-/+}$ mice, $n = 6$ APP/PS1 flox-*Prnp* Cre $^{-/-}$ mice, $n = 6$ APP/PS1 flox-*Prnp* Cre $^{-/+}$ mice. For ***I***, $n = 3$ flox-*Prnp* Cre $^{-/-}$ mice, $n = 2$ flox-*Prnp* Cre $^{-/+}$ mice, $n = 4$ APP/PS1 flox-*Prnp* Cre $^{-/-}$ mice, $n = 3$ APP/PS1 flox-*Prnp* Cre $^{-/+}$ mice.

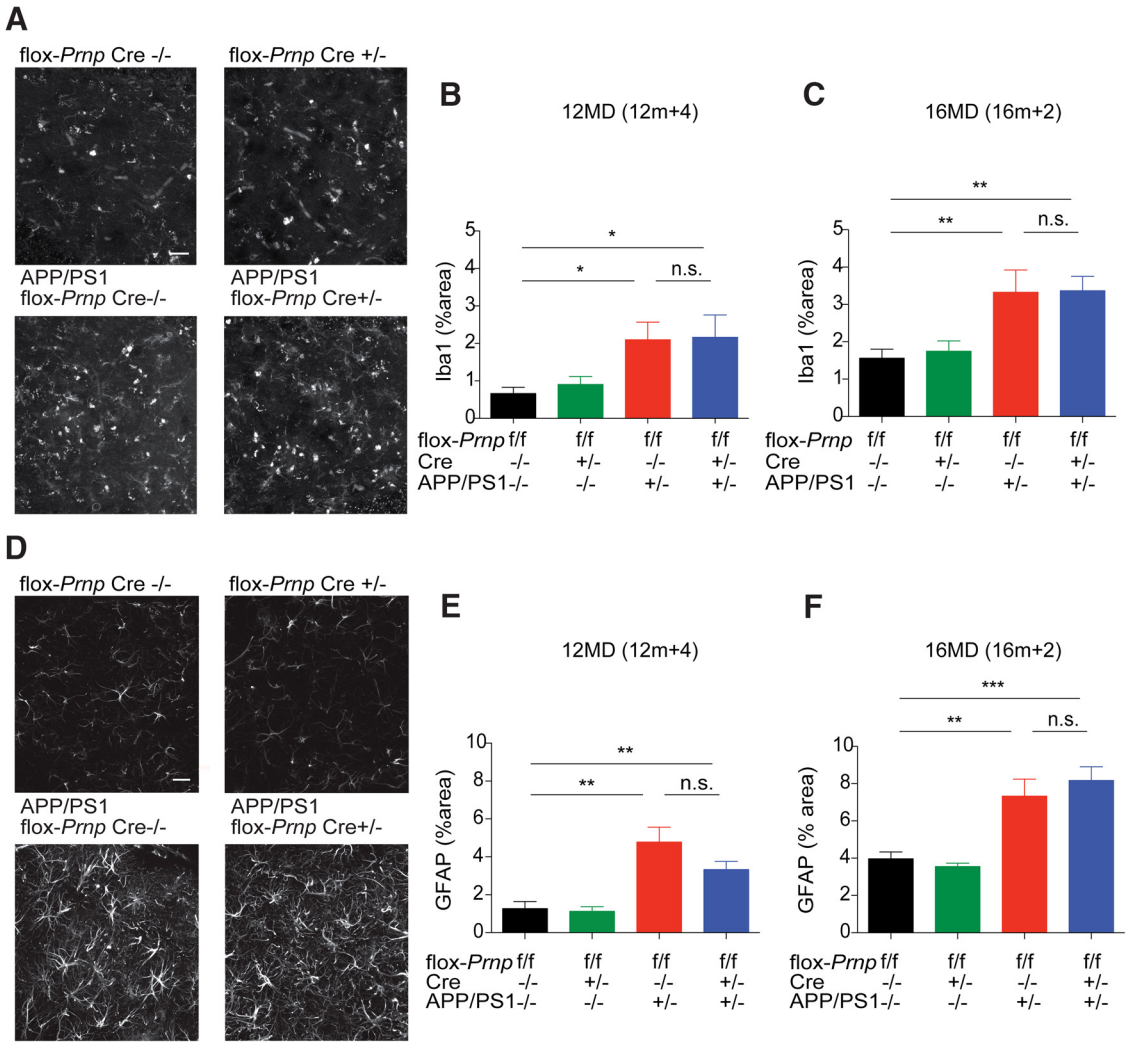

Figure 3. Deletion of *Prnp* does not have an effect on microgliosis or astrocytosis regardless of time of deletion. ***A***, Representative immunofluorescent images of the dentate gyrus stained with anti-Iba1 antibody from the 12MD cohort at 12m+4. ***B***, Quantification of Iba1-immunoreactive percentage area in the dentate gyrus for indicated genotypes from the 12MD cohort at 12m+4. Two slices per animal were analyzed. Data are graphed as mean ± SEM per animal, $n = 8$ flox-*Prnp* Cre $^{-/-}$ mice, $n = 7$ flox-*Prnp* Cre $^{-/+}$ mice, $n = 11$ APP/PS1 flox-*Prnp* Cre $^{-/-}$ mice, $n = 6$ APP/PS1 flox-*Prnp* Cre $^{-/+}$ mice. ***C***, Quantification of Iba1-immunoreactive percentage area in the dentate gyrus for the indicated genotypes from 16MD cohort at 16m+2. Two slices per animal were analyzed. Data are graphed as mean ± SEM per animal, $n = 7$ flox-*Prnp* Cre $^{-/-}$ mice, $n = 7$ flox-*Prnp* Cre $^{-/+}$ mice, $n = 6$ APP/PS1 flox-*Prnp* Cre $^{-/-}$ mice, $n = 6$ APP/PS1 flox-*Prnp* Cre $^{-/+}$ mice. In both ***B*** and ***C***, APP/PS1 flox-*Prnp* mice with or without Cre have significantly more Iba1-immunoreactive cells compared with WT controls (one-way ANOVA with uncorrected Fisher's LSD multiple-comparisons test; $^{*}p < 0.05$, $^{**}p < 0.01$). ***D***, Representative immunofluorescent images of the dentate gyrus stained with anti-GFAP antibody from the 16MD cohort at 16m+2. ***E***, Quantification of GFAP-immunoreactive percentage area in the dentate gyrus for indicated genotypes from the 12MD cohort at 12m+4. Two slices per animal were analyzed. Data are graphed as mean ± SEM per animal, $n = 8$ flox-*Prnp* Cre $^{-/-}$ mice, $n = 8$ flox-*Prnp* Cre $^{-/+}$ mice, $n = 9$ APP/PS1 flox-*Prnp* Cre $^{-/-}$ mice, $n = 6$ APP/PS1 flox-*Prnp* Cre $^{-/+}$ mice. ***F***, Quantification of GFAP-immunoreactive percentage area in the dentate gyrus for indicated genotypes from the 16MD cohort at 16m+2. Two slices per animal were analyzed. Data are graphed as mean ± SEM per animal, $n = 6$ flox-*Prnp* Cre $^{-/-}$ mice, $n = 8$ flox-*Prnp* Cre $^{-/+}$ mice, $n = 8$ APP/PS1 flox-*Prnp* Cre $^{-/-}$ mice, $n = 6$ APP/PS1 flox-*Prnp* Cre $^{-/+}$ mice. In both cohorts, APP/PS1 flox-*Prnp* mice with or without Cre have significantly more GFAP-immunoreactive cells compared with WT controls (one-way ANOVA with uncorrected Fisher's LSD multiple-comparisons test; $^{*}p < 0.05$, $^{**}p < 0.01$, $^{***}p < 0.001$). Data are graphed as mean ± SEM. Images were captured using a confocal microscope with a 40× objective. Scale bar, 20 μm.

platform removed. The start location was the point in the pool furthest from where the platform originally was placed. A reverse swim was performed with the hidden platform in a different target quadrant from the target quadrant in the forward swim. The latency to platform testing and the probe trials were recorded on a JVC Everio G-series camcorder and tracked by Panlab's Smart software.

PAT. After the administration of NOR and MWM, mice were subject to PAT using a box with equally sized, nonelectrified light and electrified dark compartments. The guillotine door between the two collapsed with the mouse's complete movement from the light to the dark side. On day one of testing, mice habituated to the light side for 90 s before the door opened. After this, the latency in seconds to enter the dark side was measured for up to 300 s. Mice received a shock lasting 2 s with an intensity of 0.5 mA on the dark side and were left in the dark for 10 s before being returned to the home cage, as described previously (Filali and Lalonde, 2009). This was repeated after 5 min for each mouse. On day two, the shock was lowered to 0 mA and the latency to enter the dark side after habituation was measured once more as a measure of retention of negative association. Perfect retention was considered the maximum latency of 5 min.

Statistics

All data are represented as means ± SEM. Prism 6 software was used for statistical analyses. All the data were analyzed by one-way or two-way ANOVA analysis as noted, followed by *post hoc* Tukey's multiple-comparisons test, Holm-0Sidak's multiple-comparisons test, and Fisher's LSD multiple-comparisons test. Two-sided tests were used and all data analyzed met the assumption for the specific statistical test used. A level of $p < 0.05$ was deemed statistically significant.

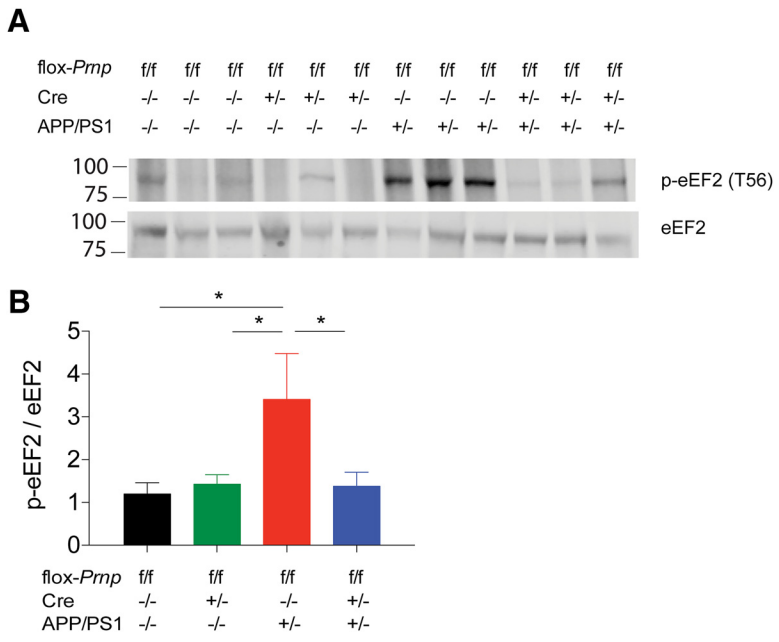

Figure 4. Activation of eEF2 is reversed by deletion of *Prnp* in the 12MD cohort. ***A***, Representative immunoblot of p-eEF2 (T56) in mice from 12MD cohort at 12m+4. Each lane represents hippocampal lysate from one mouse of the indicated genotype. Equal amount of protein loaded in each lane. ***B***, Densitometric analysis of immunoblot from ***A*** normalized to eEF2 levels. There was a significant increase in p-eEF2 (T56) levels in APP/PS1 flox-*Prnp* Cre $^{-/-}$ mice and this was reversed to WT levels in APP/PS1 flox-*Prnp* Cre $^{+/-}$ (one-way ANOVA with uncorrected Fisher's LSD test; $*p < 0.05$). Data are graphed as mean ± SEM, $n = 6$ flox-*Prnp* Cre $^{-/-}$ mice, $n = 6$ flox-*Prnp* Cre $^{-/+}$ mice, $n = 6$ APP/PS1 flox-*Prnp* Cre $^{-/-}$ mice, $n = 6$ APP/PS1 flox-*Prnp* Cre $^{-/+}$ mice.

Results

Conditional deletion reduces total PrP^C levels without inducing motor deficits or altering amyloid precursor protein (APP) metabolism

We have observed previously that constitutive deletion of PrP^C rescues many of the phenotypes associated with familial AD in mice (Laurén et al., 2009; Gimbel et al., 2010). To determine the therapeutic potential of targeting PrP^C after disease onset, we used a genetic approach to delete *Prnp* shortly after disease onset in a mouse model of familial AD (APP_{swe}/PSEN1ΔE9; hereafter referred to as APP/PS1) and months after the disease had been established. To temporally delete *Prnp*, we took advantage of mice with flox-*Prnp* alleles (Tuzi et al., 2004) and crossed these mice to mice expressing tamoxifen-inducible Cre driven ubiquitously by an actin promoter (Hayashi and McMahon, 2002). We were able to generate flox-*Prnp* Cre $^{-/-}$, flox-*Prnp* Cre $^{+/-}$, APP/PS1 flox-*Prnp* Cre $^{-/-}$, and APP/PS1 flox-*Prnp* Cre $^{+/-}$ mice on an inbred C57BL/6J background for our analysis. We established two cohorts: 12MD and 16MD (Fig. 1*H*). We performed behavioral experiments before a 3 d tamoxifen treatment and 21 d after the last day of treatment. Tamoxifen treatment was able to reduce the amount of immunoreactive PrP^C significantly (Fig. 1*A*,*B*). Furthermore, there was no difference in the degree of PrP^C reduction in males versus females (data not shown). Previous studies have shown that deletion of PrP^C can have varying developmental phenotypes depending on the insertion of the targeting construct (Rossi et al., 2001; Tuzi et al., 2004). To ensure that deletion of *Prnp* did not induce motor deficits through Doppel (*Prnd*) expression, we analyzed brain lysate from the 12MD cohort 4 months after deletion (12m + 4) and observed no evidence of Doppel expression compared with a positive testis lysate control (Fig. 1*C*). Furthermore, we did not observe motor deficits by rotarod test after ubiquitous conditional deletion of *Prnp* in the 12MD cohort (Fig. 1*D*). To determine the spatial distribution of PrP^C expression after tamoxifen treatment, we measured PrP^C expression by immunohistology using an anti-PrP^C antibody and quantified immunoreactive MFI for PrP^C in the 12MD cohort at 12m+4 (Fig. 1*E–G*). flox-*Prnp* mice positive for Cre showed a significant decrease in immunoreactive PrP^C MFI compared with Cre-negative mice independently of whether these mice expressed APP/PS1. We observed a similar level of PrP^C deletion in the stratum radiatum and the cortex and found that deletion of PrP^C using our system did not favor a subpopulation of neurons, but deleted PrP^C in a nonspecific manner. Together, these data suggest a working system for conditional deletion of PrP^C.

Previous work showed that Aβo signaling through PrP^C is downstream of APP processing and is independent of APP metabolism (Gimbel et al., 2010). To determine whether conditional deletion of *Prnp* modified APP metabolism, we measured Aβ plaque load in APP/PS1 flox-*Prnp* mice with or without Cre in both the 12MD cohort at 12m+4 (Fig. 2*A*,*B*) and 16MD cohort at 2 months after deletion (16m+2) (Fig. 2*C*,*D*) cohorts. We observed no change in Aβ plaque deposition. In addition to Aβ plaque load, we measured cortical RIPA-soluble $A\beta_{40}$ and $A\beta_{42}$ in the 12MD cohort at 12m+4 (Fig. 2*E*,*F*). We observed a significant increase in $A\beta_{40}$ and $A\beta_{42}$ levels in APP/PS1 flox-*Prnp* mice compared with WT controls, but no difference between APP/PS1 mice with or without Cre. We measured TBS-soluble $A\beta_{40}$, $A\beta_{42}$, and PrP^C-interacting Aβo in the 12MD cohort at 12m+4 (Fig. 2*G–I*). Similar to the findings in RIPA extracts, there was a significant increase in $A\beta_{40}$, $A\beta_{42}$, and PrP^C-interacting Aβo between flox-*Prnp* mice and APP/PS1 flox-*Prnp* with or without Cre. These data show that conditional deletion of *Prnp* does not alter APP metabolism.

Conditional deletion of *Prnp* does not affect microgliosis and astrocytosis

Similar to Aβ plaque load, microgliosis and astrocytosis have been shown to be separate from neuronal Aβo-PrP^C signaling and are likely driven by Aβ deposition itself (Gimbel et al., 2010). We measured gliosis by immunohistology using an anti-Iba1 antibody and quantified percentage area immunoreactive for Iba1 (Fig. 3*A–C*). APP/PS1 flox-*Prnp* mice in both cohorts showed a significant increase in Iba1-immunoreactive cells compared with WT mice and this was independent of Cre status. Similarly, we measured astrocytosis by immunohistology using an anti-GFAP antibody and quantified the percent area immunoreactive for GFAP. APP/PS1 flox-*Prnp* mice in both cohorts showed a significant increase in GFAP immunoreactivity compared with WT controls and Cre status did not change the percentage of immunoreactivity significantly (Fig. 3*D–F*). These data suggest that any synaptotoxic effects due to Aβo-PrP^C signaling are independent of microgliosis and astrocytosis.

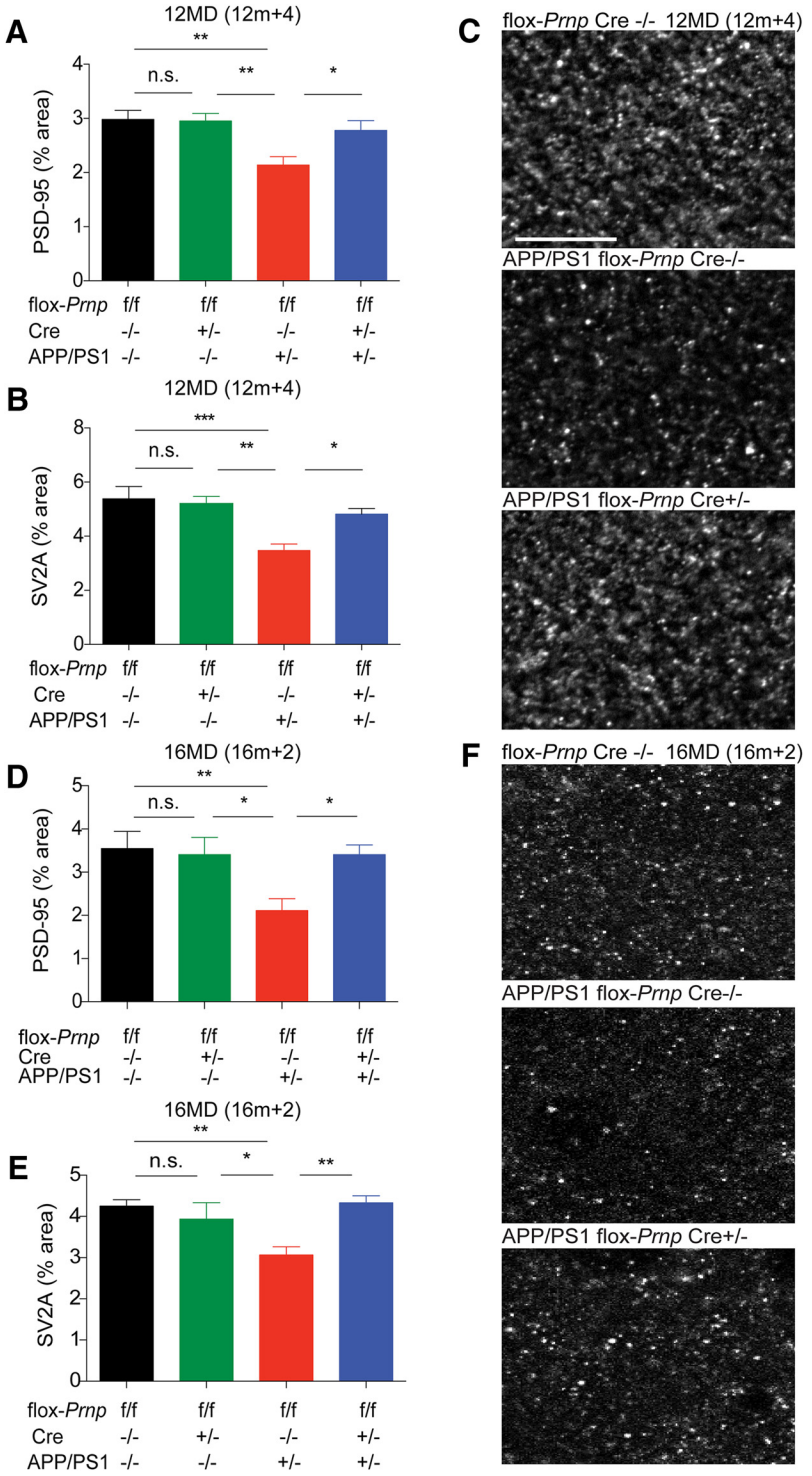

Figure 5. Synaptic density is reversed back to WT levels in APP/PS1 mice with early and late deletion of *Prnp*. ***A***, Quantification of percentage area positive with PSD-95 immunoreactivity in the dentate gyrus of the hippocampus in 12MD cohort at 12m+4. Two slices per animal were analyzed. Data are graphed as mean ± SEM per animal, $n = 10$ flox-*Prnp* Cre $^{-/-}$ mice, $n = 10$ flox-*Prnp* Cre $^{-/+}$ mice, $n = 10$ APP/PS1 flox-*Prnp* Cre $^{-/-}$ mice, $n = 10$ APP/PS1 flox-*Prnp* Cre $^{-/+}$ mice. There was a significant decrease in PSD-95 immunoreactivity in APP/PS1 flox-*Prnp* Cre $^{-/-}$ mice and this decrease was reversed in APP/PS1 flox-*Prnp* Cre $^{+/-}$ mice (one-way ANOVA with Tukey's multiple-comparisons test; $^{***}p < 0.001$, $^{**}p < 0.01$, $^{*}p < 0.05$). ***B***, Quantification of percentage area positive with SV2A immunoreactivity in the dentate gyrus of 12MD cohort at 12m+4. Two slices per animal were analyzed. Data are graphed as mean ± SEM per animal, $n = 10$ flox-*Prnp* Cre $^{-/-}$ mice, $n = 10$ flox-*Prnp* Cre $^{-/+}$ mice, $n = 10$ APP/PS1 flox-*Prnp* Cre $^{-/-}$ mice, $n = 11$ APP/PS1 flox-*Prnp* Cre $^{-/+}$ mice. There was a significant decrease in SV2A immunoreactivity in APP/PS1 flox-*Prnp* Cre $^{-/-}$ mice and this decrease was reversed in APP/PS1 flox-*Prnp* Cre $^{+/-}$ mice (one-way ANOVA with Tukey's multiple-comparisons test; $^{*}p < 0.05$). ***C***, Representative immunofluorescent images of PSD-95 immunoreactivity in the dentate gyrus of the hippocampus. Images were captured using a confocal microscope with a 63× objective. Scale bar, 10 μm. ***D***, Quantification of percentage area positive with PSD-95 immunoreactivity in the dentate gyrus of the hippocampus in the 16MD cohort at 16m+2. Two slices per animal were analyzed. Data are graphed as mean ± SEM per animal, $n = 8$ flox-*Prnp* Cre $^{-/-}$ mice, $n = 8$ flox-*Prnp* Cre $^{-/+}$ mice, $n = 8$ APP/PS1 flox-*Prnp* Cre $^{-/-}$ mice, $n = 6$ APP/PS1 flox-*Prnp* Cre $^{-/+}$ mice. There was a significant decrease in SV2A immunoreactivity in APP/PS1 flox-*Prnp* Cre $^{-/-}$ mice and this decrease was reversed in APP/PS1 flox-*Prnp* Cre $^{+/-}$ mice (one-way ANOVA with uncorrected Fisher's LSD multiple-comparisons test; $^{**}p < 0.01$, $^{*}p < 0.05$). ***E***, Quantification of percentage area positive with SV2A immunoreactivity in the dentate gyrus of 16MD cohort at 16m+2. Two slices per animal were analyzed. Data are graphed as mean ± SEM per animal, $n = 6$ flox-*Prnp* Cre $^{-/-}$ mice, $n = 6$ flox-*Prnp* Cre $^{-/+}$ mice, $n = 6$ APP/PS1 flox-*Prnp* Cre $^{-/-}$ mice, $n = 6$ APP/PS1 flox-*Prnp* Cre $^{-/+}$ mice. There was a significant decrease in SV2A immunoreactivity in APP/PS1 flox-*Prnp* Cre $^{-/-}$ mice and this decrease was reversed in APP/PS1 flox-*Prnp* Cre $^{+/-}$ mice (one-way ANOVA with uncorrected Fisher's LSD multiple-comparisons test; $^{**}p < 0.01$, $^{*}p < 0.05$). ***F***, Representative immunofluorescent images of PSD-95 immunoreactivity in the dentate gyrus of the hippocampus. Images were captured using a confocal microscope with a 63× objective.

Conditional deletion of *Prnp* reverses activated eEF2 and synapse loss in APP/PS1 mice

To further characterize temporal deletion of *Prnp*, we examined eEF2 activation in our 12MD cohort. Previous work has shown that phosphorylation of eEF2 at T56 suppresses translation and potentially mediates synaptic deficits seen in APP/PS1 mice (Horman et al., 2002; Ma et al., 2014). We harvested hippocampi from mice in the 12MD cohort at 12m+4 and found that p-eEF2 (T56) is significantly increased in the APP/PS1 flox-*Prnp* Cre $^{-/-}$, as expected, and that this increase was reversed from WT levels in the APP/PS1 flox-*Prnp* Cre $^{+/-}$ (Fig. 4). These data suggest that suppression of translation through p-eEF2 (T56) is PrP^{C} dependent and the abnormal activity can be reversed months after the disease has been established. We also observed a significant decrease by immunoblot ($p < 0.01$ by unpaired two-tailed *t* test) in Pyk2 activation from acute brain slices treated with 1 μM Aβo for 30 min from flox-*Prnp* Cre $^{-/-}$ mice (116 ± 3% of vehicle values, $n = 9$ slices from two mice) compared with flox-*Prnp* Cre $^{+/-}$ mice (99 ± 4% of vehicle values, $n = 9$ slices from two mice). Overall, conditional deletion of PrP^{C} expression normalizes Aβo-induced signal transduction.

To determine the effect of *Prnp* deletion on synapse density, we imaged synapses immunohistologically in both the 12MD cohort at 12m+4 and 16MD cohort at 16m+2. Although the same mice cannot be examined histologically at dif-

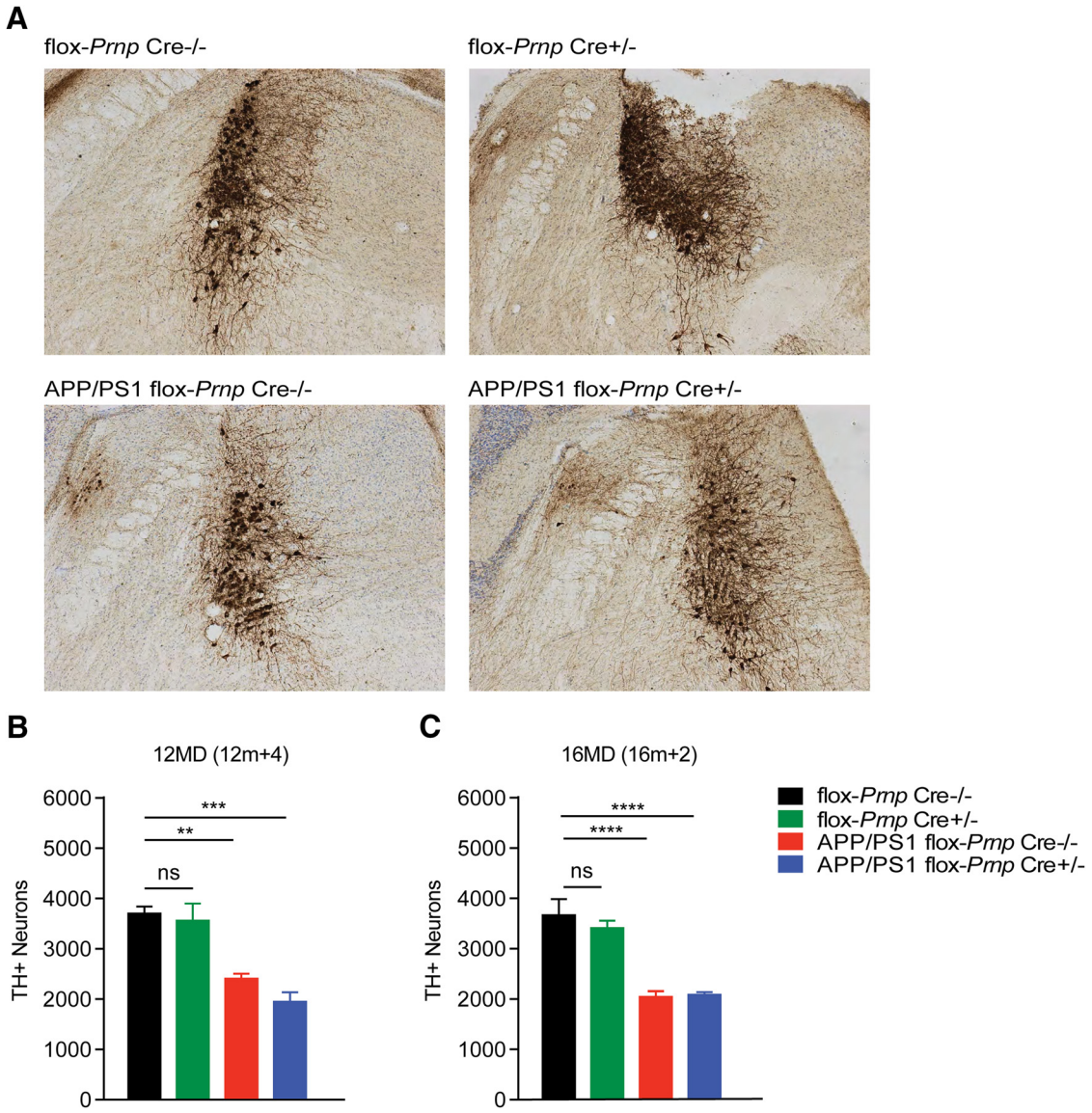

Figure 6. Deletion of *Prnp* in 12MD or 16MD cohorts did not attenuate the loss of TH-positive neurons in the LC. ***A***, Representative immunohistological images of TH immunoreactivity in the LC. Scale bar, 50 μm. ***B***, Quantification of TH-positive neurons in the 12MD cohort at 12m+4. Data are graphed as mean ± SEM, $n = 6$ flox-*Prnp* Cre $^{-/-}$ mice, $n = 7$ flox-*Prnp* Cre $^{-/+}$ mice, $n = 8$ APP/PS1 flox-*Prnp* Cre $^{-/-}$ mice, $n = 6$ APP/PS1 flox-*Prnp* Cre $^{-/+}$ mice. Both APP/PS1 groups with or without Cre displayed a significant decrease in TH-positive neurons. ***C***, Quantification of TH-positive neurons in the 16MD cohort at 16m+2. Data are graphed as mean ± SEM, $n = 8$ flox-*Prnp* Cre $^{-/-}$ mice, $n = 9$ flox-*Prnp* Cre $^{-/+}$ mice, $n = 8$ APP/PS1 flox-*Prnp* Cre $^{-/-}$ mice, $n = 4$ APP/PS1 flox-*Prnp* Cre $^{-/+}$ mice. Both APP/PS1 groups with or without Cre displayed a similar significant decrease in TH-positive neurons. Both APP/PS1 groups in both cohorts displayed ~a 50% decrease of TH-positive LC neurons compared with non-APP/PS1 littermate controls as shown by two-way ANOVA (**$p < 0.01$; ***$p < 0.001$; ns, nonsignificant).

ferent ages, our previous studies (Park et al., 2006; Gimbel et al., 2010; Um et al., 2012, 2013; Haas et al., 2016; Kaufman et al., 2015; Nygaard et al., 2015) clearly showed reduced synapse density in this strain by 12 months of age. We stained brain sections using anti-PSD-95 (postsynaptic marker) or anti-SV2A (presynaptic marker) antibodies. Synapse density in the APP/PS1 flox-*Prnp* Cre $^{-/-}$ group at 12m+4 displayed a significant decrease as percentage of area immunoreactive for PSD-95 and SV2A (Fig. 5*A–C*). Conversely, synapse density in APP/PS1 flox-*Prnp* Cre $^{+/-}$ mice was rescued to WT levels (Fig. 5*A–C*). Further, the 16MD cohort at 16m+2 also displayed a significant decrease in synapse density by PSD-95 and SV2A immunoreactivity in the APP/PS1 flox-*Prnp* Cre $^{-/-}$ group (Fig. 5*D–F*) and this deficit was fully restored in the APP/PS1 flox-*Prnp* Cre $^{+/-}$ group to WT levels (Fig. 5*D–F*). Therefore, the decrease in synapse density seen in the APP/PS1 mice is PrP^{C} dependent and conditional deletion of *Prnp* is able to reverse this deficit even after the disease has been fully established.

Conditional deletion of *Prnp* at 12 and 16 months fails to reverse monoaminergic degeneration

Although synapses can recover after conditional gene deletion, other aspects of neuronal degeneration may be either irreversible or PrP^{C} independent. Degeneration of monoaminergic neurons has been described in the APP/PS1 mice, starting before 12 months and progressing through 18 months (Liu et al., 2008). Constitutive PrP^{C} deletion rescued early serotonin fiber loss in the cerebral cortex (Gimbel et al., 2010). Here, we assessed TH-positive neurons in the LC for the groups with *Prnp* deletion at 12m+4 (12MD) and 16m+2 (16MD) months (Fig. 6). Stereological counts of TH-positive neurons were decreased by nearly 50% in the APP/PS1 mice regardless of the conditional PrP^{C} loss.

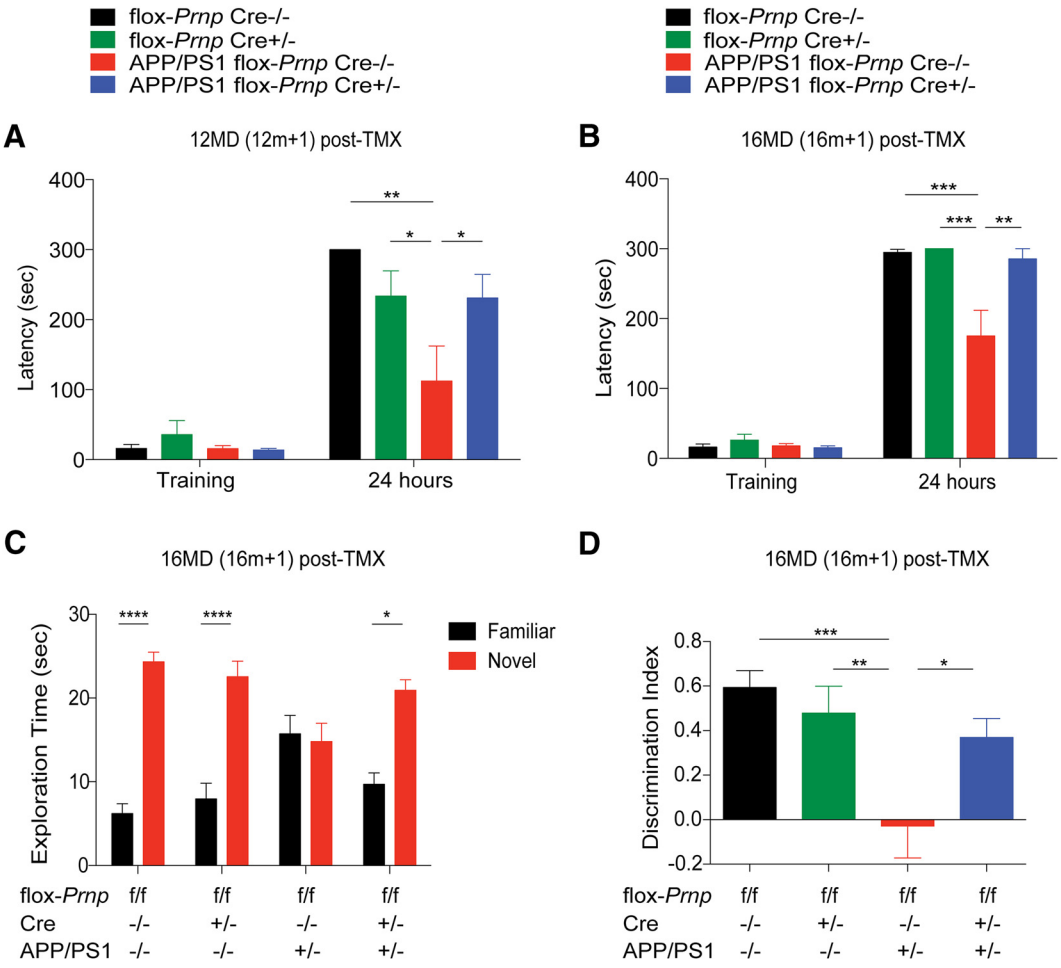

Figure 7. Deletion of *Prnp* during early and late disease state is able to reverse behavioral deficits in PAT and NOR. ***A***, 12MD cohort at 12m+1 was subjected to PAT after Cre activation through tamoxifen treatment. All animals were treated with tamoxifen regardless of genotype. APP/PS1 flox-*Prnp* Cre $^{-/-}$ mice showed a significant decrease in latency to enter the dark chamber, whereas the APP/PS1 flox-*Prnp* Cre $^{+/-}$ mice had a significant increase in latency similar to that of WT mice (two-way ANOVA with Holm–Sidak's multiple-comparisons test; ***$p < 0.001$, **$p < 0.01$, *$p < 0.05$). Data are graphed as mean ± SEM, $n = 5$ flox-*Prnp* Cre $^{-/-}$ mice, $n = 8$ flox-*Prnp* Cre $^{-/+}$ mice, $n = 5$ APP/PS1 flox-*Prnp* Cre $^{-/-}$ mice, $n = 9$ APP/PS1 flox-*Prnp* Cre $^{-/+}$ mice. ***B***, 16MD cohort at 16m+1 was subjected to PAT after Cre activation through tamoxifen treatment. All animals were treated with tamoxifen regardless of genotype. APP/PS1 flox-*Prnp* Cre $^{-/-}$ mice showed a significant decrease in latency to enter the dark chamber, whereas the APP/PS1 flox-*Prnp* Cre $^{+/-}$ mice had a significant increase in latency similar to that of WT mice (two-way ANOVA with Holm–Sidak's multiple-comparisons test; ***$p < 0.001$, **$p < 0.01$). Data are graphed as mean ± SEM, $n = 11$ flox-*Prnp* Cre $^{-/-}$ mice, $n = 12$ flox-*Prnp* Cre $^{-/+}$ mice, $n = 10$ APP/PS1 flox-*Prnp* Cre $^{-/-}$ mice, $n = 5$ APP/PS1 flox-*Prnp* Cre $^{-/+}$ mice. ***C***, 16MD cohort at 16m+1 was subjected to NOR. All animals were treated with tamoxifen regardless of genotype. The mice were familiarized to an object and subsequently allowed to explore both a familiar or novel object. APP/PS1 flox-*Prnp* Cre $^{-/-}$ mice did not display a preference for either object, whereas APP/PS1 flox-*Prnp* Cre $^{+/-}$ mice showed a significant preference for the novel object similar to WT mice (two-way ANOVA with Holm–Sidak's multiple-comparisons test; ***$p < 0.001$, *$p < 0.05$). Data are graphed as mean ± SEM, $n = 11$ flox-*Prnp* Cre $^{-/-}$ mice, $n = 12$ flox-*Prnp* Cre $^{-/+}$ mice, $n = 10$ APP/PS1 flox-*Prnp* Cre $^{-/-}$ mice, $n = 6$ APP/PS1 flox-*Prnp* Cre $^{-/+}$ mice. ***D***, Discrimination index for ***C*** was calculated as follows: (novel − familiar)/(novel + familiar). APP/PS1 flox-*Prnp* Cre $^{-/-}$ mice displayed a discrimination index close to zero, whereas APP/PS1 flox-*Prnp* Cre $^{+/-}$ mice showed a significant increase in their discrimination index similar to WT mice (one-way ANOVA with uncorrected Fisher's LSD test; ****$p < 0.0001$, ***$p < 0.001$, **$p < 0.01$, *$p < 0.05$).

Therefore, this phenotype does not require continued expression of PrP^C.

Conditional deletion of *Prnp* at 12 and 16 months is able to rescue behavioral deficits

To investigate whether deletion of *Prnp* of at 12 (12MD) and 16 (16MD) months could reverse familial AD phenotypes in our mouse model, we assessed both cohorts before and after deletion of *Prnp* (Fig. 1*D*). We performed PAT only after tamoxifen treatment on the 12MD cohort at 12m+1 and the 16MD cohort at 16m+1 due to the inability to repeat this training procedure in the same mice. We did not find a difference in latency during the training portion, but observed that APP/PS1 flox-*Prnp* Cre $^{-/-}$ have a significant decrease in latency to enter the dark chamber after 24 h (Fig. 7*A*,*B*). Deletion of *Prnp* in APP/PS1 flox-*Prnp* Cre $^{+/-}$ mice at either 12m (Fig. 7*A*) or 16m (Fig. 7*B*) was able to prevent fully this behavioral deficit at 12m+1 and 16m+1, respectively. These data suggest that deletion of *Prnp* at 12 months and at 16 months, is able to rescue behavioral deficits seen in PAT.

To evaluate a distinct learning paradigm, we performed the NOR test on the 16MD cohort at 16m+1. WT mice with or without Cre preferred the familiar object, whereas APP/PS1 flox-*Prnp* Cre $^{-/-}$ mice did not have an object preference (Fig. 7*C*). Deletion of *Prnp* in the APP/PS1 flox-*Prnp* Cre $^{+/-}$ group generated a preference for the novel object similar to WT mice (Fig. 7*C*). The discrimination index, reflecting the difference in object exploration times, was close to zero for the APP/PS1 flox-*Prnp* Cre $^{-/-}$ mice, whereas the APP/PS1 flox-*Prnp* Cre $^{+/-}$ and WT mice with or without Cre showed a similar positive discrimination index (Fig. 7*D*). Together, these data show that deletion of *Prnp* after disease onset is able to reverse behavioral PAT deficits

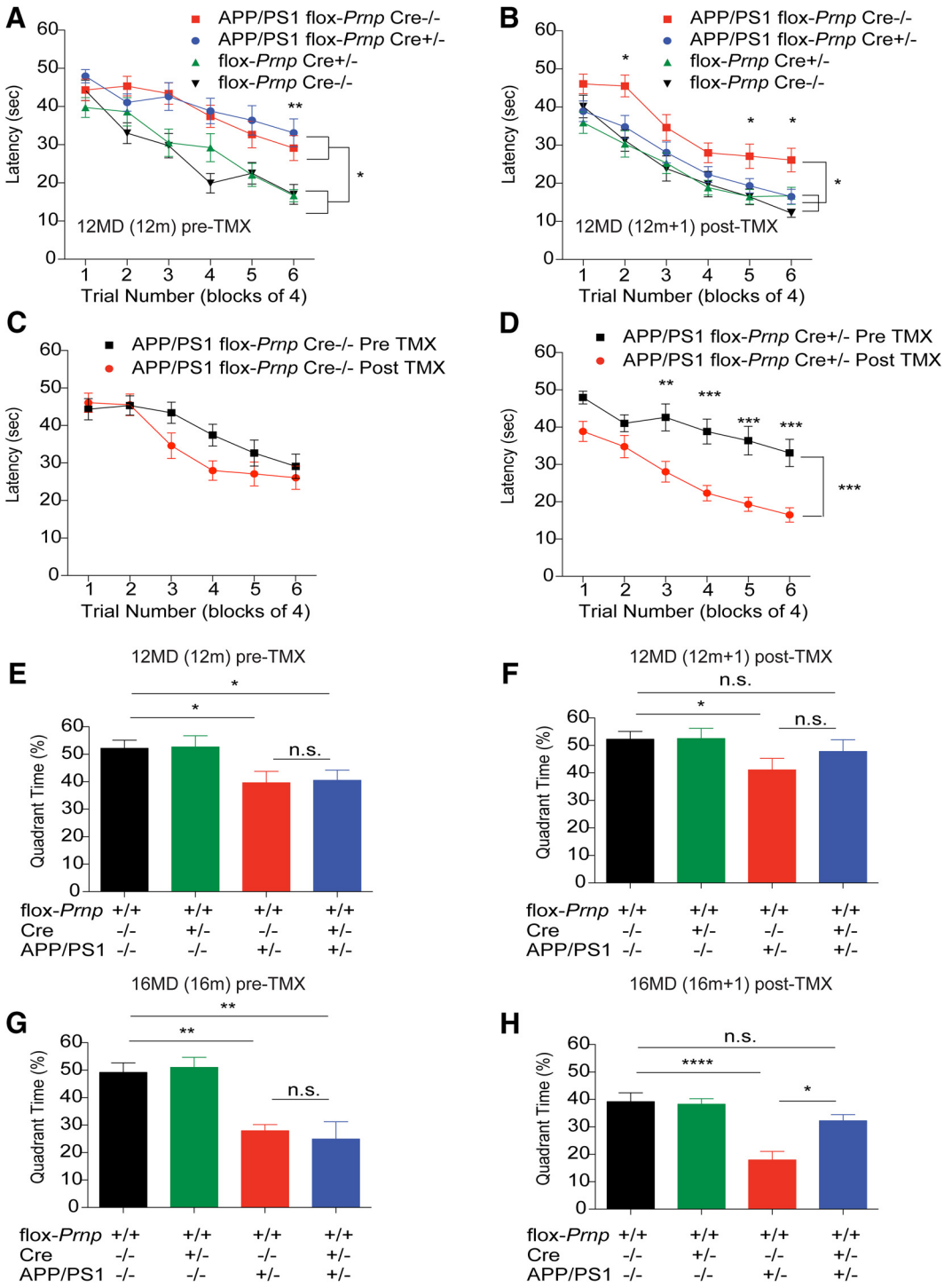

Figure 8. Deletion of *Prnp* during early and late disease state is able to reverse learning and memory deficits in MWM. ***A***, 12MD cohort at 12m+1 was subjected to MWM and latency was calculated as time to find a hidden platform. The forward swim was performed on mice before Cre activation. Both APP/PS1 mice with or without the Cre gene had a significantly higher latency compared with WT controls in the last four swims (two-way RM-ANOVA; APP/PS1 flox *Prnp* Cre $^{-/-}$ and APP/PS1 flox *Prnp* Cre $^{+/-}$, $^{**}p < 0.01$). Data are graphed as mean ± SEM, $n = 21$ flox-*Prnp* Cre $^{-/-}$ mice, $n = 21$ flox-*Prnp* Cre $^{-/+}$ mice, $n = 20$ APP/PS1 flox-*Prnp* Cre $^{-/-}$ mice, $n = 20$ APP/PS1 flox-*Prnp* Cre $^{-/+}$ mice. ***B***, Cre was activated with a 3 d tamoxifen treatment. The reverse swim was performed 21 d after the last day of tamoxifen treatment. APP/PS1 flox-*Prnp* Cre $^{-/-}$ mice had significantly higher latency compared with APP/PS1 flox-*Prnp* Cre $^{+/-}$ and WT mice in the last eight swims (two-way RM-ANOVA; APP/PS1 flox *Prnp* Cre $^{+/-}$, $^{*}p < 0.05$). Data are graphed as mean ± SEM, $n = 16$ flox-*Prnp* Cre $^{-/-}$ mice, $n = 17$ flox-*Prnp* Cre $^{-/+}$ mice, $n = 17$ APP/PS1 flox-*Prnp* Cre $^{-/-}$ mice, $n = 15$ APP/PS1 flox-*Prnp* Cre $^{-/+}$ mice. ***C***, Data from ***A*** with the latency from the APP/PS1 flox-*Prnp* Cre $^{-/-}$ group separated into pre-tamoxifen (black) and post-tamoxifen (red). Latency of either group was not statistically significant. ***D***, Data from ***B*** with the latency from the APP/PS1 flox-*Prnp* Cre $^{+/-}$ group separated into pre-tamoxifen (black) and post-tamoxifen (red). APP/PS1 flox-*Prnp* Cre $^{+/-}$ mice are able to learn significantly better after Cre activation (two-way RM-ANOVA; APP/PS1 flox *Prnp* Cre $^{+/-}$ pre-tamoxifen, $^{**}p < 0.01$, $^{***}p < 0.001$). ***E***, The probe trial was performed from the cohort in ***A*** after trial 6 by removing the hidden platform. Quadrant time percentage is quantified as the amount of time spent in the target quadrant in 1 min. APP/PS1 flox *Prnp* mice with or without Cre spent significantly less time in the target quadrant compared with WT (one-way ANOVA with uncorrected Fisher's LSD test; $^{*}p < 0.05$). ***F***, This probe trial was performed from the same group in ***B*** after trial 6. WT groups spent significantly more time in the target quadrant compared with APP/PS1 groups (one-way ANOVA with uncorrected Fisher's LSD test; $^{*}p < 0.05$). Although not significant compared with the APP/PS1 flox-*Prnp* Cre $^{-/-}$ group, the APP/PS1 flox-*Prnp* Cre $^{+/-}$ group spent a similar amount of time in the target quadrant after Cre activation as WT mice. ***G***, Similar to the cohort in ***E***, the probe trial was performed in the 16MD cohort at 16m+1 after trial 6 by removing (*Figure legend continues.*)

and reversal of behavioral deficits in NOR and PAT is achieved even when *Prnp* deletion occurs many months after the disease has been established.

To further examine learning and memory in our model, we performed MWM on both cohorts. We analyzed the 12MD cohort before and after deletion of *Prnp*. We performed the first set of 24 training swims (six blocks of four swims) to a hidden platform in the 12MD cohort at 12 months. The APP/PS1 flox-*Prnp* groups with or without Cre had a significantly higher latency to find the hidden platform than did the WT groups (Fig. 8*A*). We performed a second set of training swims to a hidden platform in a different quadrant of the pool 21 d after a 3 d tamoxifen treatment (12m+1). In contrast to the first swim set, the post-TMX behavior of the APP/PS1 flox-*Prnp* Cre $^{+/-}$ group showed significantly reduced time to the hidden platform, whereas the APP/PS1 flox-*Prnp* Cre $^{-/-}$ group did not improve (Fig. 8*B*). As shown in Figure 8*C*, for mice without Cre and thus no Cre-mediated deletion of *Prnp*, the second training session was as poor as the first. Conversely, the APP/PS1 flox-*Prnp* Cre $^{+/-}$ mice exhibited significantly better learning of the platform after tamoxifen treatment (Fig. 8*D*). A probe trial was performed 24 h after trial block six. The APP/PS1 flox-*Prnp* groups with or withour Cre before tamoxifen treatment spent significantly less time in the target quadrant compared with WT groups with or without Cre (Fig. 8*E*). After the second training set (after tamoxifen treatment), the APP/PS1 flox-*Prnp* Cre $^{-/-}$ mice spent less time in the target quadrant, similar to the first probe trial, whereas APP/PS1 flox-*Prnp* Cre $^{+/-}$ mice showed a trend to spent more time in the target quadrant (Fig. 8*F*). We also assessed *Prnp* deletion later during disease progression in the 16MD cohort at 16m and 16m+1. For this group, during the pre-tamoxifen session, the APP/PS1 flox-*Prnp* mice with or without Cre spent significantly less time in the target quadrant compared with WT mice with or without Cre (Fig. 8*G*). After tamoxifen treatment at 16 months, the APP/PS1 flox-*Prnp* Cre $^{+/-}$ spent just as much time as WT mice in the target quadrant and significantly more time compared with APP/PS1 flox-*Prnp* Cre $^{-/-}$ mice still expressing PrP^{C} (Fig. 8*H*). Together, these data demonstrate that *Prnp* deletion can reverse synaptotoxic effects on learning and memory mediated by Aβo-PrP^{C} signaling during early and late stages of disease progression.

Discussion

The major finding in our study is that deletion of *Prnp* after disease onset reverses synaptic and behavioral deficits in a mouse model of familial AD. Specifically, temporally controlled deletion of *Prnp* during early onset of the disease at 12 months of age and after continued progression of the disease at 16 months of age can reverse behavioral deficits. Our system provides slightly less than complete loss of *Prnp*, but the widespread substantial reduction of PrP^{C} expression is sufficient to reverse a decrease in synaptic density and behavioral deficits in a mouse model of familial AD. This work confirms and extends our previous study using a constitutive deletion model of PrP^{C} (Gimbel et al., 2010; Haas et al., 2016). Importantly, this work underscores the clinical potential of targeting PrP^{C} for two reasons: (1) we have shown that PrP^{C} deletion can be efficacious after disease onset and (2) we have shown that less than total deletion of *Prnp* is sufficient for reversal of AD related phenotypes. Partial deletion holds greater clinical relevance because it is doubtful that any pharmacological intervention can achieve 100% blockade. Combined, these data suggest that reduction of PrP^{C} can reverse AD-associated phenotypes in a transgenic mouse model.

As an artifact of the gene targeting, the *Prnp*-related gene Doppel is aberrantly expressed in certain mouse models. The CNS expression of Doppel from *Prnp* regulatory elements leads to Purkinje cell loss and ataxia (Rossi et al., 2001). Using our tamoxifen-inducible system, we have shown that Doppel expression remains unchanged before and after Cre activation. Therefore, these mice do not exhibit locomotor dysfunction by rotarod test or display behavioral abnormalities by several paradigms for learning and memory. We have shown that this *Prnp* deletion model does not display any obvious phenotype and can be used for Aβo-PrP^{C} related studies with temporal control of PrP^{C} expression.

Our previous work suggests that PrP^{C} is required for synaptic and behavioral deficits seen in a mouse model of AD (Gimbel et al., 2010; Haas et al., 2016). Similarly, we have found that conditional deletion of <100% of *Prnp* is sufficient to reverse the same synaptic and behavioral deficits long after disease onset. In addition, conditional deletion of *Prnp* does not change Aβ plaque burden, RIPA- or TBS-soluble Aβ, or PrP^{C}-interacting Aβo, suggesting that the Aβo–PrP^{C} interaction is downstream of APP metabolism. Furthermore, we did not observe a significant effect on astrocytosis or microgliosis through *Prnp* deletion, suggesting that the Aβo-PrP^{C} effects are neuron specific. Further work is necessary to fully determine whether these effects are cell autonomous within neurons. We observed that eEF2 phosphorylation was reversed, supporting previous work (Um et al., 2013; Ma et al., 2014; Haas et al., 2016; Kaufman et al., 2015) that suppressed protein translation in this familial AD mouse model is PrP^{C} dependent. Overall, these findings confirm the hypothesis that late suppression of most PrP^{C} expression achieves the near complete rescue observed with constitutive and complete ablation.

Multiple receptors for Aβ oligomers have been reported in addition to PrP^{C} (for review, see Smith and Strittmatter, 2017). The data reported here indicate that PrP^{C} is required for the continued presence of behavioral and synaptic deficits in APP/PS1 mice. Previous evidence from us and others have shown that PrP^{C} is a major receptor for Aβo (Laurén et al., 2009; Chen et al., 2010; Dohler et al., 2014). To the extent that other receptors are required in addition to PrP^{C} with regard to manifestation of these phenotypes, they must be co-dependent with PrP^{C}. Work from Kostylev et al. (2015) suggests the precise nature of Aβo species vary from model to model and alternate transgenic models may be more dependent on other receptors. The current study demonstrates the genetic dependence of APP/PS1 phenotypes on the continued presence of PrP^{C}, but they are not designed to explore whether it is acting specifically as a receptor or by an unknown indirect mechanism. Given previous work, a receptor explanation is the most parsimonious, but we cannot formally exclude the possibility that indirect mechanisms may contribute.

Synapse area is restored by PrP^{C} deletion in aged APP/PS1 mice. This goes beyond simply arresting further damage and im-

←

(*Figure legend continued.*) the hidden platform. Before tamoxifen treatment, APP/PS1 flox-*Prnp* mice with or without Cre spent significantly less time in the target quadrant compared with WT controls (one-way ANOVA with Tukey's multiple-comparisons test; $^{**}p < 0.01$). Data are graphed as mean ± SEM, $n = 13$ flox-*Prnp* Cre $^{-/-}$ mice, $n = 12$ flox-*Prnp* Cre $^{-/+}$ mice, $n = 9$ APP/PS1 flox-*Prnp* Cre $^{-/-}$ mice, $n = 7$ APP/PS1 flox-*Prnp* Cre $^{-/+}$ mice. ***H***, After Cre activation through tamoxifen treatment, APP/PS1 flox-*Prnp* Cre $^{+/-}$ mice spent significantly more time in the target quadrant compared with APP/PS1 flox-*Prnp* Cre $^{-/-}$ mice (one-way ANOVA with Tukey's multiple-comparisons test; $^{*}p < 0.05$, $^{****}p < 0.0001$, $^{*}p < 0.05$). Data are graphed as mean ± SEM, $n = 10$ flox-*Prnp* Cre $^{-/-}$ mice, $n = 5$ flox-*Prnp* Cre $^{-/+}$ mice, $n = 11$ APP/PS1 flox-*Prnp* Cre $^{-/-}$ mice, $n = 12$ APP/PS1 flox-*Prnp* Cre $^{-/+}$ mice.

plies that new synapses can be formed in the adult mouse brain if pathological processes are blocked. Techniques have been developed to monitor synapse stability *in vivo* with transgenic markers and two photon imaging (Holtmaat and Svoboda, 2009). These methods have shown that, whereas many synapses are stable, new synapses are formed in the adult mouse brain even at advanced age (Mostany et al., 2013). We have documented adult brain synapse formation previously in aged APP/PS1 mice (Heiss et al., 2017). Therefore, if an intervention can block those mechanisms that are accelerating synapse loss in an AD model, then the existing literature provides a basis for expecting synapse restoration (Um et al., 2013; Kaufman et al., 2015).

Although synaptic loss is reversible and synapse density is fully restored by late *Prnp* deletion, catecholaminergic degeneration in the LC is not. This degeneration may occur by PrP^C-independent mechanisms. Our previous observation of cortical serotonin axon rescue in constitutive *Prnp* mice at 12 months suggests that at least early degeneration for 5HT neurons is PrP^C dependent-(Gimbel et al., 2010). Conversely, rescue of neurodegeneration may require more complete removal of PrP^C than is achieved by the conditional paradigm. Another alternative is that, once monoaminergic degeneration is under way, it cannot be reversed in the same way that the synaptic deficits are by PrP^C removal. The relative role of temporal versus dose-dependent versus molecular distinctions in the resistance of monoaminergic neurons to the benefit of conditional *Prnp* deletion will require further investigation.

AD is primarily a disease of learning and memory and, accordingly, we were able to measure the effect of *Prnp* deletion on APP/PS1-dependent learning and memory phenotypes in our mouse model. Importantly, we observed that partial deletion was sufficient to reverse behavioral deficits whether gene knock-out occurred shortly after disease onset or many months later, when behavioral and anatomical deficits are robust. We observed robust learning and memory deficits by MWM in all APP/PS1 groups before tamoxifen treatment when *Prnp* remained intact. One month after tamoxifen treatment, this learning and memory deficit was rescued in the same mice that previously displayed this deficit. The reversal of synapse density provides an explanation for this functional recovery. We observed a similar result when we deleted *Prnp* at 12 or 16 months. Similarly, we observed a rescue of memory impairment in NOR test and PAT after tamoxifen treatment. The broader implications of this study suggest that targeting the Aβo–PrP^C interaction after disease onset can be beneficial. Nevertheless, it remains unclear how late *Prnp* can be deleted and still provide therapeutic efficacy and if the moment of irreversibility is due to chronic downstream signals induced through Aβo-PrP^C signaling.

In contrast to targeting the downstream effects of Aβ, numerous studies have focused on decreasing the amount of Aβ burden by using tet-off gene-regulatable systems. Researchers were able to reduce Aβ levels to WT levels by suppressing mutant $APP_{Swe/Ind}$ in a transgenic mouse model using doxycycline administration (Jankowsky et al., 2005). Their system successfully reduced Aβ levels, but demonstrated that early suppression of $APP_{Swe/Ind}$ was necessary because amyloid plaques were slow to clear once deposited. Suppression of this transgenic APP during early postnatal development rescued locomotor hyperactivity (Rodgers et al., 2012) and a separate study using 12- to 13-month-old mice with a similar tet-off gene-regulatable system found that suppressing transgenic APP expression was able to rescue impairments in both short- and long-term memory tasks (Melnikova et al., 2013). Although this study suggested that suppression of APP on the order of weeks was enough to reverse cognitive deficits seen in this mouse model of familial AD (FAD), it remained unclear whether soluble Aβ species or plaques were responsible. Fowler et al. (2014) were able to show that 2-week suppression of APP using the same tet-off gene-regulatable system was able to partially rescue short-term learning and memory deficits, whereas plaque burden remained unchanged, suggesting that a soluble form of Aβ was responsible for this rescue. Using our conditional deletion system, we also saw a reversibility of endophenotypes associated with our mouse model of FAD, suggesting that, at least in part, cognitive deficits seen in FAD mouse models is mediated by the Aβo–PrP^C interaction.

Here, we demonstrate reversibility of a number of AD-related phenotypes in a transgenic mouse model. Deletion of *Prnp* at either 12 or 16 months was able to reverse synaptic and behavioral deficits seen in this transgenic AD model. Even though the conditional deletion of *Prnp* was partial, this was sufficient to reverse fully synaptic and behavioral phenotypes. This work supports clinical translation of PrP^C targeting for AD treatment. Importantly, it suggests that inhibiting the Aβo-PrP^C interaction during later stages of disease will be efficacious. Although PrP^C targeting fully reverses synapse loss when cell loss is minimal in the APP/PS1 mouse model, its efficacy in the clinical situation might be predicted to shift from reversing early deficits dependent on synapse dysfunction to slowing progression in advanced stages when cell loss is substantial. Given the high rate of failure for AD directed therapies (Cummings et al., 2014), PrP^C is a promising candidate given its cell surface location and potential for small-molecule-directed therapeutics. Nevertheless, further research is required to better understand Aβo–PrP^C signaling and to develop disease-modifying therapeutics for the treatment of AD.

References

Aimi T, Suzuki K, Hoshino T, Mizushima T (2015) Dextran sulfate sodium inhibits amyloid-beta oligomer binding to cellular prion protein. J Neurochem 134:611–617. CrossRef Medline

Alzheimer's Association (2012) 2012 Alzheimer's disease facts and figures. Alzheimers Dement 8:131–168. CrossRef Medline

Balducci C, Beeg M, Stravalaci M, Bastone A, Sclip A, Biasini E, Tapella L, Colombo L, Manzoni C, Borsello T, Chiesa R, Gobbi M, Salmona M, Forloni G (2010) Synthetic amyloid-beta oligomers impair long-term memory independently of cellular prion protein. Proc Natl Acad Sci U S A 107:2295–2300. CrossRef Medline

Barry AE, Klyubin I, Mc Donald JM, Mably AJ, Farrell MA, Scott M, Walsh DM, Rowan MJ (2011) Alzheimer's disease brain-derived amyloid-beta-mediated inhibition of LTP in vivo is prevented by immunotargeting cellular prion protein. J Neurosci 31:7259–7263. CrossRef Medline

Braak H, Braak E (1991) Neuropathological staging of Alzheimer-related changes. Acta Neuropathol 82:239–259. CrossRef Medline

Bradford BM, Tuzi NL, Feltri ML, McCorquodale C, Cancellotti E, Manson JC (2009) Dramatic reduction of PrP C level and glycosylation in peripheral nerves following PrP knock-out from Schwann cells does not prevent transmissible spongiform encephalopathy neuroinvasion. J Neurosci 29:15445–15454. CrossRef Medline

Calella AM, Farinelli M, Nuvolone M, Mirante O, Moos R, Falsig J, Mansuy IM, Aguzzi A (2010) Prion protein and Abeta-related synaptic toxicity impairment. EMBO Mol Med 2:306–314. CrossRef Medline

Chen S, Yadav SP, Surewicz WK (2010) Interaction between human prion protein and amyloid-beta (Abeta) oligomers: role OF N-terminal residues. J Biol Chem 285:26377–26383. CrossRef Medline

Chung E, Ji Y, Sun Y, Kascsak RJ, Kascsak RB, Mehta PD, Strittmatter SM, Wisniewski T (2010) Anti-PrPC monoclonal antibody infusion as a novel treatment for cognitive deficits in an Alzheimer's disease model mouse. BMC Neurosci 11:130. CrossRef Medline

Cummings JL, Morstorf T, Zhong K (2014) Alzheimer's disease drug-development pipeline: few candidates, frequent failures. Alzheimers Res Ther 6:37. CrossRef Medline

Dohler F, Sepulveda-Falla D, Krasemann S, Altmeppen H, Schlüter H, Hildebrand D, Zerr I, Matschke J, Glatzel M (2014) High molecular mass assemblies of amyloid-beta oligomers bind prion protein in patients with Alzheimer's disease. Brain 137:873–886. CrossRef Medline

Filali M, Lalonde R (2009) Age-related cognitive decline and nesting behavior in an APPswe/PS1 bigenic model of Alzheimer's disease. Brain Res 1292:93–99. CrossRef Medline

Fluharty BR, Biasini E, Stravalaci M, Sclip A, Diomede L, Balducci C, La Vitola P, Messa M, Colombo L, Forloni G, Borsello T, Gobbi M, Harris DA (2013) An N-terminal fragment of the prion protein binds to amyloid-beta oligomers and inhibits their neurotoxicity in vivo. J Biol Chem 288: 7857–7866. CrossRef Medline

Fowler SW, Chiang AC, Savjani RR, Larson ME, Sherman MA, Schuler DR, Cirrito JR, Lesne SE, Jankowsky JL (2014) Genetic modulation of soluble Aβ rescues cognitive and synaptic impairment in a mouse model of Alzheimer's disease. J Neurosci 34:7871–7885. CrossRef

Freir DB, Nicoll AJ, Klyubin I, Panico S, Mc Donald JM, Risse E, Asante EA, Farrow MA, Sessions RB, Saibil HR, Clarke AR, Rowan MJ, Walsh DM, Collinge J (2011) Interaction between prion protein and toxic amyloid beta assemblies can be therapeutically targeted at multiple sites. Nat Commun 2:336. CrossRef Medline

Gimbel DA, Nygaard HB, Coffey EE, Gunther EC, Laurén J, Gimbel ZA, Strittmatter SM (2010) Memory impairment in transgenic Alzheimer mice requires cellular prion protein. J Neurosci 30:6367–6374. CrossRef Medline

Haas LT, Salazar SV, Kostylev MA, Um JW, Kaufman AC, Strittmatter SM (2016) Metabotropic glutamate receptor 5 couples cellular prion protein to intracellular signalling in Alzheimer's disease. Brain 139:526–546. CrossRef Medline

Hardy J, Selkoe DJ (2002) The amyloid hypothesis of Alzheimer's disease: progress and problems on the road to therapeutics. Science 297:353–356. CrossRef Medline

Hayashi S, McMahon AP (2002) Efficient recombination in diverse tissues by a tamoxifen-inducible form of Cre: a tool for temporally regulated gene activation/inactivation in the mouse. Dev Biol 244:305–318. CrossRef Medline

Heiss JK, Barrett J, Yu Z, Haas LT, Kostylev MA, Strittmatter SM (2017) Early activation of experience-independent dendritic spine turnover in a mouse model of Alzheimer's disease. Cereb Cortex 7:3660–3674.

Holtmaat A, Svoboda K (2009) Experience-dependent structural synaptic plasticity in the mammalian brain. Nat Rev Neurosci 10:647–658. CrossRef Medline

Horman S, Browne G, Krause U, Patel J, Vertommen D, Bertrand L, Lavoinne A, Hue L, Proud C, Rider M (2002) Activation of AMP-activated protein kinase leads to the phosphorylation of elongation factor 2 and an inhibition of protein synthesis. Curr Biol 12:1419–1423. CrossRef Medline

Hu NW, Nicoll AJ, Zhang D, Mably AJ, O'Malley T, Purro SA, Terry C, Collinge J, Walsh DM, Rowan MJ (2014) mGlu5 receptors and cellular prion protein mediate amyloid-beta-facilitated synaptic long-term depression in vivo. Nat Commun 5:3374. CrossRef Medline

Jankowsky JL, Slunt HH, Gonzales V, Savonenko AV, Wen JC, Jenkins NA, Copeland NG, Younkin LH, Lester HA, Younkin SG, Borchelt DR (2005) Persistent amyloidosis following suppression of Abeta production in a transgenic model of Alzheimer disease. PLoS Med 2:e355. CrossRef Medline

Kaufman AC, Salazar SV, Haas LT, Yang J, Kostylev MA, Jeng AT, Robinson SA, Gunther EC, van Dyck CH, Nygaard HB, Strittmatter SM (2015) Fyn inhibition rescues established memory and synapse loss in Alzheimer mice. Ann Neurol 77:953–971. CrossRef Medline

Kessels HW, Nguyen LN, Nabavi S, Malinow R (2010) The prion protein as a receptor for amyloid-beta. Nature 466:E3–4; discussion E4–5. CrossRef Medline

Klyubin I, Nicoll AJ, Khalili-Shirazi A, Farmer M, Canning S, Mably A, Linehan J, Brown A, Wakeling M, Brandner S, Walsh DM, Rowan MJ, Collinge J (2014) Peripheral administration of a humanized anti-PrP antibody blocks Alzheimer's disease Abeta synaptotoxicity. J Neurosci 34:6140–6145. CrossRef Medline

Kostylev MA, Kaufman AC, Nygaard HB, Patel P, Haas LT, Gunther EC, Vortmeyer A, Strittmatter SM (2015) Prion-protein-interacting amyloid-beta oligomers of high molecular weight are tightly correlated with memory impairment in multiple Alzheimer mouse models. J Biol Chem 290:17415–17438. CrossRef Medline

Lambert MP, Barlow AK, Chromy BA, Edwards C, Freed R, Liosatos M, Morgan TE, Rozovsky I, Trommer B, Viola KL, Wals P, Zhang C, Finch CE, Krafft GA, Klein WL (1998) Diffusible, nonfibrillar ligands derived from Abeta1–42 are potent central nervous system neurotoxins. Proc Natl Acad Sci U S A 95:6448–6453. CrossRef Medline

Larson M, Sherman MA, Amar F, Nuvolone M, Schneider JA, Bennett DA, Aguzzi A, Lesné SE (2012) The complex PrP(c)-Fyn couples human oligomeric Abeta with pathological tau changes in Alzheimer's disease. J Neurosci 32:16857–16871a. CrossRef Medline

Laurén J, Gimbel DA, Nygaard HB, Gilbert JW, Strittmatter SM (2009) Cellular prion protein mediates impairment of synaptic plasticity by amyloid-beta oligomers. Nature 457:1128–1132. CrossRef Medline

Lesné S, Koh MT, Kotilinek L, Kayed R, Glabe CG, Yang A, Gallagher M, Ashe KH (2006) A specific amyloid-beta protein assembly in the brain impairs memory. Nature 440:352–357. CrossRef Medline

Liu Y, Yoo MJ, Savonenko A, Stirling W, Price DL, Borchelt DR, Mamounas L, Lyons WE, Blue ME, Lee MK (2008) Amyloid pathology is associated with progressive monoaminergic neurodegeneration in a transgenic mouse model of Alzheimer's disease. J Neurosci 28:13805–13814. CrossRef Medline

Ma T, Chen Y, Vingtdeux V, Zhao H, Viollet B, Marambaud P, Klann E (2014) Inhibition of AMP-activated protein kinase signaling alleviates impairments in hippocampal synaptic plasticity induced by amyloid beta. J Neurosci 34:12230–12238. CrossRef Medline

Mayeux R (2003) Epidemiology of neurodegeneration. Annu Rev Neurosci 26:81–104. CrossRef Medline

Melnikova T, Fromholt S, Kim H, Lee D, Xu G, Price A, Moore BD, Golde TE, Felsenstein KM, Savonenko A, Borchelt DR (2013) Reversible pathologic and cognitive phenotypes in an inducible model of Alzheimer-amyloidosis. J Neurosci 33:3765–3779. CrossRef Medline

Mölsä PK, Marttila RJ, Rinne UK (1986) Survival and cause of death in Alzheimer's disease and multi-infarct dementia. Acta Neurol Scand 74: 103–107. Medline

Mostany R, Anstey JE, Crump KL, Maco B, Knott G, Portera-Cailliau C (2013) Altered synaptic dynamics during normal brain aging. J Neurosci 33:4094–4104. CrossRef Medline

Nygaard HB, Kaufman AC, Sekine-Konno T, Huh LL, Going H, Feldman SJ, Kostylev MA, Strittmatter SM (2015) Brivaracetam, but not ethosuximide, reverses memory impairments in an Alzheimer's disease mouse model. Alzheimers Res Ther 7:25. CrossRef Medline

Osborne C, West E, Nolan W, McHale-Owen H, Williams A, Bate C (2016) Glimepiride protects neurons against amyloid-beta-induced synapse damage. Neuropharmacology 101:225–236. CrossRef Medline

Park JH, Widi GA, Gimbel DA, Harel NY, Lee DH, Strittmatter SM (2006) Subcutaneous Nogo receptor removes brain amyloid-beta and improves spatial memory in Alzheimer's transgenic mice. J Neurosci 26:13279–13286. CrossRef Medline

Rodgers SP, Born HA, Das P, Jankowsky JL (2012) Transgenic APP expression during postnatal development causes persistent locomotor hyperactivity in the adult. Mol Neurodegener 7:28. CrossRef Medline

Rossi D, Cozzio A, Flechsig E, Klein MA, Rülicke T, Aguzzi A, Weissmann C (2001) Onset of ataxia and Purkinje cell loss in PrP null mice inversely correlated with Dpl level in brain. EMBO J 20:694–702. CrossRef Medline

Rushworth JV, Griffiths HH, Watt NT, Hooper NM (2013) Prion protein-mediated toxicity of amyloid-beta oligomers requires lipid rafts and the transmembrane LRP1. J Biol Chem 288:8935–8951. CrossRef Medline

Scheff SW, Price DA, Schmitt FA, Mufson EJ (2006) Hippocampal synaptic loss in early Alzheimer's disease and mild cognitive impairment. Neurobiol Aging 27:1372–1384. CrossRef Medline

Schnell SA, Staines WA, Wessendorf MW (1999) Reduction of lipofuscin-like autofluorescence in fluorescently labeled tissue. J Histochem Cytochem 47:719–730. CrossRef Medline

Selkoe DJ (2002) Alzheimer's disease is a synaptic failure. Science 298:789–791. CrossRef Medline

Selkoe DJ (2011) Alzheimer's disease. Cold Spring Harb Perspect Biol 3: pii: a004457. CrossRef Medline

Shankar GM, Li S, Mehta TH, Garcia-Munoz A, Shepardson NE, Smith I, Brett FM, Farrell MA, Rowan MJ, Lemere CA, Regan CM, Walsh DM, Sabatini BL, Selkoe DJ (2008) Amyloid-beta protein dimers isolated di-

rectly from Alzheimer's brains impair synaptic plasticity and memory. Nat Med 14:837–842. CrossRef Medline

Sheng M, Sabatini BL, Sudhof TC (2012) Synapses and Alzheimer's disease. Cold Spring Harb Perspect Biol 4: pii: a005777. CrossRef

Smith LM, Strittmatter SM (2017) Binding sites for amyloid-beta oligomers and synaptic toxicity. Cold Spring Harb Perspect Med 7: pii: a024075. CrossRef Medline

Tuzi NL, Clarke AR, Bradford B, Aitchison L, Thomson V, Manson JC (2004) Cre-loxP mediated control of PrP to study transmissible spongiform encephalopathy diseases. Genesis 40:1–6. CrossRef Medline

Um JW, Nygaard HB, Heiss JK, Kostylev MA, Stagi M, Vortmeyer A, Wisniewski T, Gunther EC, Strittmatter SM (2012) Alzheimer amyloid-beta oligomer bound to postsynaptic prion protein activates Fyn to impair neurons. Nat Neurosci 15:1227–1235. CrossRef Medline

Um JW, Kaufman AC, Kostylev M, Heiss JK, Stagi M, Takahashi H, Kerrisk ME, Vortmeyer A, Wisniewski T, Koleske AJ, Gunther EC, Nygaard HB, Strittmatter SM (2013) Metabotropic glutamate receptor 5 is a coreceptor for Alzheimer abeta oligomer bound to cellular prion protein. Neuron 79:887–902. CrossRef Medline

Walsh DM, Klyubin I, Fadeeva JV, Cullen WK, Anwyl R, Wolfe MS, Rowan MJ, Selkoe DJ (2002) Naturally secreted oligomers of amyloid beta protein potently inhibit hippocampal long-term potentiation in vivo. Nature 416:535–539. CrossRef Medline

Yiannopoulou KG, Papageorgiou SG (2013) Current and future treatments for Alzheimer's disease. Ther Adv Neurol Disord 6:19–33. CrossRef Medline

Zhang H, Wu L, Pchitskaya E, Zakharova O, Saito T, Saido T, Bezprozvanny I (2015) Neuronal store-operated calcium entry and mushroom spine loss in amyloid precursor protein knock-in mouse model of Alzheimer's disease. J Neurosci 35:13275–13286. CrossRef Medline

Zhang R, Xue G, Wang S, Zhang L, Shi C, Xie X (2012) Novel object recognition as a facile behavior test for evaluating drug effects in AbetaPP/PS1 Alzheimer's disease mouse model. J Alzheimers Dis 31:801–812. CrossRef Medline

Vol 457|26 February 2009|doi:10.1038/nature07761

LETTERS

Cellular prion protein mediates impairment of synaptic plasticity by amyloid-β oligomers

Juha Laurén[1], David A. Gimbel[1], Haakon B. Nygaard[1], John W. Gilbert[1] & Stephen M. Strittmatter[1]

A pathological hallmark of Alzheimer's disease is an accumulation of insoluble plaque containing the amyloid-β peptide of 40–42 amino acid residues[1]. Prefibrillar, soluble oligomers of amyloid-β have been recognized to be early and key intermediates in Alzheimer's-disease-related synaptic dysfunction[2–9]. At nanomolar concentrations, soluble amyloid-β oligomers block hippocampal long-term potentiation[7], cause dendritic spine retraction from pyramidal cells[5,8] and impair rodent spatial memory[2]. Soluble amyloid-β oligomers have been prepared from chemical syntheses, transfected cell culture supernatants, transgenic mouse brain and human Alzheimer's disease brain[2,4,7,9]. Together, these data imply a high-affinity cell-surface receptor for soluble amyloid-β oligomers on neurons—one that is central to the pathophysiological process in Alzheimer's disease. Here we identify the cellular prion protein (PrP^C) as an amyloid-β-oligomer receptor by expression cloning. Amyloid-β oligomers bind with nanomolar affinity to PrP^C, but the interaction does not require the infectious PrP^{Sc} conformation. Synaptic responsiveness in hippocampal slices from young adult PrP null mice is normal, but the amyloid-β oligomer blockade of long-term potentiation is absent. Anti-PrP antibodies prevent amyloid-β-oligomer binding to PrP^C and rescue synaptic plasticity in hippocampal slices from oligomeric amyloid-β. Thus, PrP^C is a mediator of amyloid-β-oligomer-induced synaptic dysfunction, and PrP^C-specific pharmaceuticals may have therapeutic potential for Alzheimer's disease.

To characterize amyloid-β-oligomer-binding sites, we synthesized amyloid-β(1–42) peptide conjugated to biotin through the α amino group (biotin–Aβ42), and then denatured the peptide and allowed oligomers to form as described for amyloid-β-derived diffusible ligands[4]. Consistent with findings for untagged Aβ42 oligomers[5], biotin–Aβ42-oligomer preparations contain spherical particles of 5–6 nm in diameter visible by negative staining with transmission electron microscopy, with rare protofibrils and no larger fibrils (Fig. 1a). Approximately 50% of the peptide migrates by size-exclusion chromatography (SEC) as a distinct assembly with a size of approximately 500 kDa corresponding to 50–100 amyloid-β monomers (Fig. 1b). Low-molecular-weight forms of Aβ42 in either oligomeric or fresh preparations migrate by SEC as monomers (Fig. 1b), demonstrating that the trimers or tetramers observed by SDS–polyacrylamide gel electrophoresis (Supplementary Fig. 1) are not present under native conditions[10]. Aβ42 oligomer binds to hippocampal neurons, whereas freshly prepared biotin–Aβ42 does not (Fig. 1c and Supplementary Fig. 2). Biotin–Aβ42-oligomer binding is enriched in MAP2 (also known as MTAP2)-positive dendrites, with lower levels in βIII-tubulin (TUBB3)-positive axons, and very low levels in astroglial cells (Supplementary Fig. 3a, c, data not shown and ref. 6). The Aβ42-oligomer binding is most concentrated at post-synaptic densities marked by immunoreactive PSD-95 (also known as DLG4; Supplementary Fig. 3b). Binding to neurons is saturable, with an apparent dissociation constant (K_d) of 50–100 nM monomer equivalent (Fig. 1d). The K_d of the relevant Aβ42 assembly must be much less than 100 nM because minimal binding is detected with freshly prepared Aβ42. If the Aβ42 species responsible for binding contains 100 monomers and represents 50% of all biotin–Aβ42 in the preparation, the corrected affinity would be ~0.4 nM. Although this formulation of Aβ42 oligomer is not chromatographically identical to the Aβ42 oligomer from brain[2,3,9], it affords detection of high-affinity binding sites likely to share pathological actions with sites for other Aβ42-oligomer preparations[5,6,11].

A key requirement for expression cloning of Aβ42-oligomer-binding sites is the existence of a cell line with low background binding. COS-7 cells exhibit <5% of the biotin–Aβ42-oligomer binding level in hippocampal neurons. We expressed complementary DNAs from an adult mouse brain library in COS-7 cells and screened for biotin–Aβ42-oligomer binding. From 225,000 clones, 2 independent positive clones were isolated and both were found to encode full-length mouse PrP (Fig. 1e). Aβ42 oligomers bind to cells expressing the PrP^C conformation; interaction is not dependent on the PrP^{Sc} conformation required for infectious prion disease[12]. PrP^C is known to interact with copper ion but this does not alter Aβ42-oligomer binding (Supplementary Fig. 4). Like hippocampal neurons, PrP^C-expressing COS-7 cells have much lower affinity for freshly prepared low-molecular-weight biotin–Aβ42 (Fig. 1e and Table 1). The apparent dissociation constant for biotin–Aβ42-oligomer binding to PrP^C-expressing COS-7 cells is indistinguishable from that for biotin–Aβ42-oligomer binding to hippocampal neurons (Fig. 1f, g and Table 1). The selectivity of PrP for binding Aβ42 oligomer versus fresh Aβ42 is reflected in the ratio of K_d values and must be greater than 20 (>2,000 nM/92 nM) based on the total peptide monomer concentration in the Aβ42-oligomer preparation (Table 1), or as great as 5,000 (>2,000 nM/0.4 nM) based on the molar concentration of Aβ42 oligomer estimated by SEC/light scattering (LS) (Fig. 1b).

To explore any contribution of the biotin tag to PrP affinity, we prepared untagged Aβ42 oligomer and examined binding to PrP^C-expressing cells with an anti-amyloid-β antibody (Supplementary Fig. 5). Untagged Aβ42 binding is localized to PrP^C-expressing cells. Thus, binding is mediated by the amyloid-β amino acid residues. The simplest model for PrP^C expression inducing Aβ42-oligomer binding is a direct interaction between the two polypeptides. To verify this, we examined the interaction of purified PrP–Fc with Aβ42 (Supplementary Fig. 6). A control Fc protein, immobilized on a resin, retained neither freshly prepared nor oligomeric preparations of Aβ42. In contrast, PrP–Fc protein retained Aβ42 peptide through a direct physical interaction. The pre-incubated oligomeric form of Aβ42 was retained to a 2.5-fold greater degree than the freshly prepared peptide. The preference of PrP for amyloid-β oligomer versus fresh Aβ42 is less complete here than in the cellular assays, perhaps owing to the use of concentrated solid-phase purified reagents and higher concentrations.

[1]Cellular Neuroscience, Neurodegeneration and Repair Program, Yale University School of Medicine, New Haven, Connecticut 06536, USA.

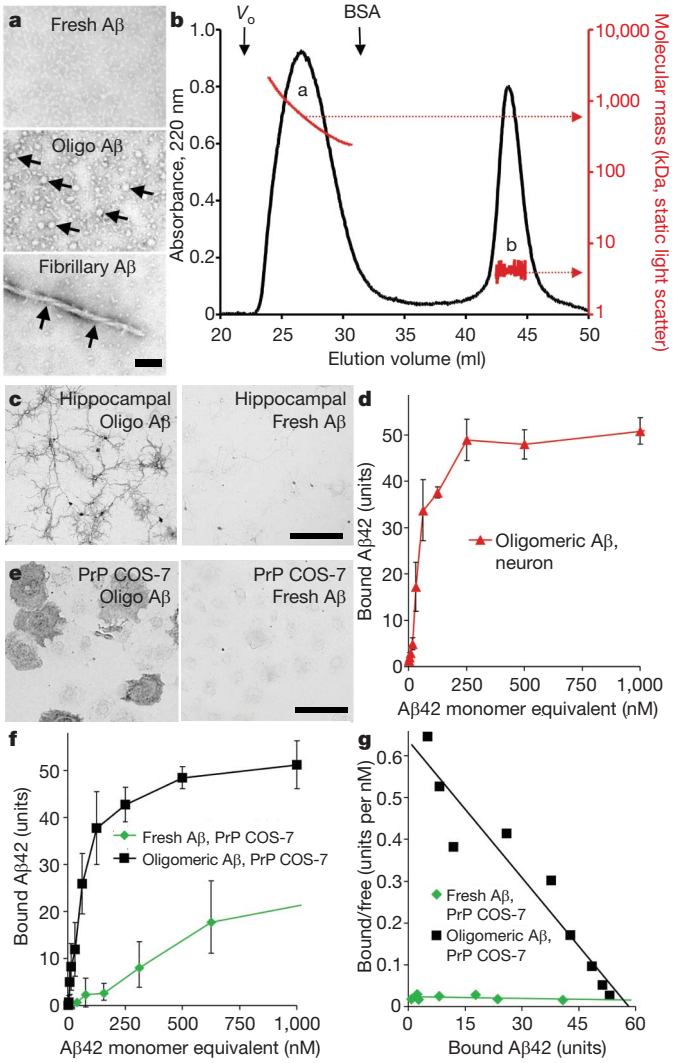

Figure 1 | Oligomeric Aβ42 binds to neurons and to cells expressing PrP^C. **a**, Freshly prepared, oligomeric or fibrillary preparations of Aβ42 were examined by transmission electron microscopy with negative staining. The arrows indicate globular oligomers in the middle segment and a fibril in the lower segment. Aβ, amyloid-β. Scale bar, 25 nm. **b**, Oligomeric Aβ42 peptide was analysed by SEC, monitoring absorbance at 220 nm (black) and light scattering (red). The void volume (V_o) and elution of bovine serum albumin (BSA) from a separate run are shown. Peak 'a' is oligomeric Aβ42 and 'b' is monomeric Aβ42. **c**, Oligomeric Aβ42 peptide (200 nM total peptide) binds to 21 DIV hippocampal neurons (left), whereas fresh Aβ42 (200 nM) does not (right). Bound biotin–Aβ42 was visualized by alkaline-phosphatase-conjugated streptavidin. **d**, Dose-dependence of oligomeric Aβ42 binding to hippocampal neurons. **e**, The binding of 40 nM oligomeric or freshly prepared Aβ42 to COS-7 cells expressing PrP^C. **f**, **g**, Fresh or oligomeric Aβ42 binding to PrP^C-expressing COS-7 cells as a function of Aβ42 total concentration (monomer equivalent for oligomer preparations). Data are mean ± s.e.m., and the Scatchard analysis is presented in **g**. Scale bars, 100 μm for **c** and **e**.

Although the PrP cDNA is the only clone to support oligomeric Aβ42 binding isolated from the brain cDNA library, we considered whether other amyloid-β-binding sites might exist. First, we examined two clones sharing sequence similarity with PrP—doppel (also known as PRND) and SPRN—but neither showed affinity for oligomeric Aβ42 (Table 1 and Supplementary Fig. 7). Second, we screened a pre-existing collection of 352 cDNAs encoding transmembrane proteins one by one. In this format, weaker affinity interactions are detectable than in the initial pooled brain library screen. Amyloid-β precursor-like protein 1 (APLP1) and transmembrane protein 30B (TMEM30B) were isolated through this focused screen and demonstrate K_d values for oligomeric Aβ42 of 660 nM and 720 nM, respectively (Table 1 and Supplementary Fig. 7). These lower affinity binding proteins exhibit limited specificity for oligomeric Aβ42, as compared to fresh Aβ42. APLP1 shares similarity with amyloid-β precursor protein (APP) and with APLP2, but neither of these proteins binds Aβ42 (Table 1). TMEM30B is similar to TMEM30A, which is expressed at high levels in the brain. TMEM30A supports Aβ42 binding with an affinity similar to TMEM30B and shows no preference for oligomeric species (Table 1). The receptor for advanced glycation end products (RAGE) and the α7 nicotinic acetylcholine receptor (nAChRα7, also known as CHRNA7) have been reported to bind amyloid-β[13,14]. In this heterologous COS-7 cell binding assay, expression of RAGE yielded less Aβ42-oligomer-binding signal than did PrP, APLP1 or TMEM30B, and we failed to detect binding to nAChRα7 (Supplementary Fig. 7). Thus, although several proteins exhibit Aβ42 binding, only PrP has high affinity and high selectivity for the oligomeric peptide.

Binding of Aβ42 oligomer to neurons depends on the developmental stage, with minimal binding to neurons immediately after dissociation from E18 hippocampus. Binding of Aβ42 oligomer to neurons does not become robust until 15–20 days have elapsed *in vitro* (Fig. 2a). The immunoblot level of PrP^C expression closely matches this developmental pattern (Fig. 2b). Immunocytochemically, PrP^C expression is largely restricted to MAP2-positive dendrites of differentiated neurons (Supplementary Fig. 3d and Fig. 2c). Furthermore, localization of PrP immunoreactivity and Aβ42-oligomer binding overlap extensively (Fig. 2c). If PrP^C (encoded by *Prnp*) were the only cellular binding site for Aβ42 oligomers, then no binding would be detected in cultures from *Prnp*$^{-/-}$ mice at 20 days *in vitro* (DIV). Because we observe 50% reduction of punctate Aβ42-oligomer binding in such cultures (Fig. 2d, e), PrP^C cannot be the only cell-surface molecule binding Aβ42 oligomers. Multiple alternative sites, including APLP1, TMEM30A, TMEM30B, RAGE and unidentified proteins, may explain Aβ42 binding to *Prnp*$^{-/-}$ neurons.

Different domains of PrP^C have been associated with various activities. The amino-terminal octapeptide repeat domain (amino acids 60–95) contributes to extracellular copper ion binding[15,16]. The unstructured central domain (amino acids 95–134) includes a charge cluster (amino acids 95–110) and a segment with hydrophobic character (amino acids 112–134). This central domain has been implicated in masking a neurodegenerative activity of PrP^C (refs 17 and 18). The carboxy-terminal domain is globular (amino acids 134–231)[19] and the protein is glycosyl phosphatidylinositol (GPI)-anchored to the plasma membrane. We mapped Aβ42-oligomer binding using PrP deletion mutants (Fig. 3). Each mutant protein was expressed at the COS-7 surface by live anti-PrP immunostaining (Fig. 3a and Supplementary Fig. 8). Deletion of the octapeptide repeat domain and the central domain (Δ32–121) abrogates binding, indicating that the globular domain alone cannot mediate binding. The hydrophobic 105–125 region is not a major determinant, because Δ105–125 protein binds Aβ42 oligomers indistinguishably from full-length PrP^C, and because the Δ32–106 variant behaves like the Δ32–121 variant, having no Aβ42-oligomer affinity. To distinguish whether the 95–110 charge cluster or the octapeptide repeat domain is crucial for Aβ42 binding, a mutant lacking the 52–91 segment was expressed. The Δ52–91 mutant exhibits significant Aβ42 binding, implicating the 95–110 region as a principal site for Aβ42-oligomer binding. Consistent with this hypothesis, deletion of 11 amino acids in the Δ95–105 variant reduced binding by 80%, and there was no further reduction in the Δ70–105 variant.

As an alternative method to localize Aβ42 binding within PrP^C, we used anti-PrP antibodies (Fig. 3b–d). Of the six antibodies initially tested, only one (6D11) blocked the binding of Aβ42 assemblies to PrP^C, and did so with a half-maximal inhibitory concentration of 1 nM (Fig. 3b–d and Supplementary Figs 8–10). The 6D11 blockade is epitope-specific because the 7D9 antibody binds avidly to a different epitope but fails to block Aβ42 binding (Fig. 3a–d and Supplementary Figs 8 and 9). The epitope for 6D11 corresponds to amino acids 93–109 of mouse PrP^C, matching the conclusion that the 95–105 amino

Table 1 | Aβ42 binding to COS-7 cells expressing the indicated proteins

Surface protein	Clone source	Oligomer amyloid-β K_d (nM)*	Fresh amyloid-β K_d (nM)*	Oligomer selectivity†
PrP	225,000 brain cDNAs	92 ± 14	>2,000‡	>21
SPRN	Similar to PrP	>2,000‡	>2,000‡	
doppel	Similar to PrP	>2,000	>2,000	
APLP1	352 transmembrane	660 ± 30	>2,000‡	>3
APLP2	Similar to APLP1	>2,000	>2,000	
APP	Similar to APLP1	>2,000	>2,000	
TMEM30A	Similar to TMEM30B	990 ± 60	1,100 ± 60	1.1
TMEM30B	352 transmembrane	720 ± 20	870 ± 70	1.2

APLP1 and TMEM30B were identified by examination of individual clones from a 352-member pre-existing collection of expression vectors for transmembrane proteins (Origene).
* K_d values are mean ± s.e.m. and are based on monomer equivalent concentrations.
† Oligomer selectivity is the ratio of the monomer K_d to the oligomer K_d.
‡ Binding of Aβ42 was detected at 2 μM ligand, but binding was not saturated.

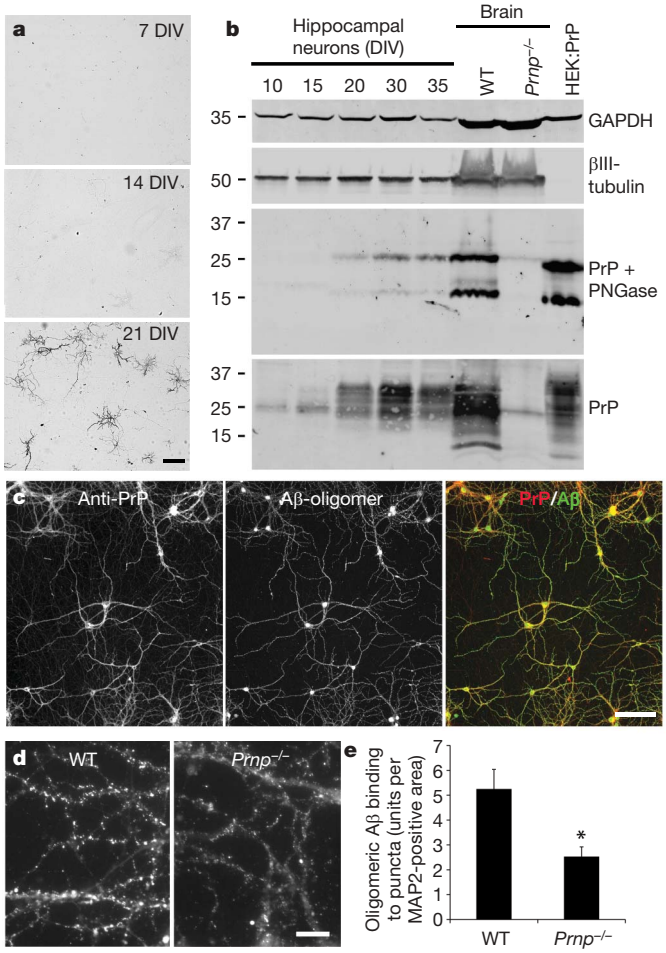

Figure 2 | Characterization of Aβ42 oligomer binding sites. a, Oligomeric Aβ42 (30 nM) binding to hippocampal neurons after culture for the indicated time. Neuronal cell density is similar in the three panels. Scale bar, 100 μm. **b**, Total protein (20 μg) from hippocampal cultures, from whole brain of the indicated genotype or from HEK293T cells transfected with a PrP expression vector was analysed by immunoblot with anti-PrP antibody (8H4), with anti-βIII-tubulin antibody or with anti-GAPDH antibody. Samples for the middle panel were pretreated with endoglycosidase (PNGase F) before gel electrophoresis through a 4–20% polyacrylamide gel in Tris-glycine-SDS. Molecular weight standards are shown at the left in kDa. **c**, Hippocampal neurons from E18 mice after 21 DIV were incubated with biotinylated Aβ42 oligomer (130 nM monomer equivalent) for 1 h at 37 °C and then fixed. Bound amyloid-β was detected with fluorescent avidin (green), and PrP^C with anti-PrP immunocytochemistry (red). Scale bar, 100 μm. **d**, Cultures were prepared from wild-type (WT) or $Prnp^{-/-}$ mice, and then binding of Aβ42-oligomer (130 nM monomer equivalent) was detected as in **c**. Scale bar, 10 μm. **e**, Binding of 100 nM Aβ42 oligomers to puncta in hippocampal cultures as shown in **d**. Data from $n = 6$ pairs of cultures from wild-type and $Prnp^{-/-}$ embryos. Mean and s.e.m.; $^*P < 0.05$, two-tailed t-test.

acid region is a primary determinant for binding. To confirm this hypothesis, we examined the effect of an additional antibody (8G8) with an overlapping epitope, amino acids 95–110. The 8G8 antibody blocked the Aβ42–PrP^C interaction, although with a lesser potency than 6D11. The effect of 6D11 was not caused by internalization of PrP^C, because similar cell-surface levels of PrP^C were detectable after 6D11 pre-incubation (Supplementary Fig. 11). The 6D11 antibody is highly specific for PrP^C, as no immunoreactivity was observed in *Prnp* null brain sections nor was there any reactivity to Aβ42 (Supplementary Fig. 12 and not shown). We conclude that the 95–105 segment of PrP^C contributes to Aβ42-oligomer binding in a 6D11-sensitive manner.

Although these data demonstrate that PrP^C is a high-affinity binding site for Aβ42 oligomers, they do not assess its role in the pathological actions of Aβ42. It has been noted that soluble Aβ42 oligomers suppress long-term potentiation (LTP) of the Schaffer collateral pathway between hippocampal CA3 and CA1 pyramidal cells[7,11]. Therefore, we compared the effects of soluble Aβ42 oligomers on LTP from slices of wild-type versus $Prnp^{-/-}$ mice[20,21]. As reported previously, soluble Aβ42 oligomers (500 nM total peptide, estimated 2 nM Aβ42 oligomer) reduce LTP in hippocampal slices from wild-type mice (Fig. 4a, d). The slope of the excitatory postsynaptic potential (EPSP) after theta burst stimulation is augmented by 80% in control slices, but only by 20% in slices pre-incubated with Aβ42-oligomer preparations. In slices from 2–6-month-old PrP null mice without Aβ42 treatment, Schaffer collateral LTP is indistinguishable from baseline levels of wild-type mice (Fig. 4b), as described previously[22,23]. Notably, there is no inhibition of LTP by Aβ42 oligomers in the $Prnp^{-/-}$ slices (Fig. 4b–d).

The lack of Aβ42 sensitivity for LTP in $Prnp^{-/-}$ slices indicates that PrP^C acts as a receptor for Aβ42 oligomers mediating inhibition of LTP in wild-type slices. Alternatively, chronic loss of PrP^C may lead to developmental and/or compensatory effects that account indirectly for Aβ42 oligomer ineffectiveness. To separate these possibilities, we pretreated wild-type slices with the 6D11 anti-PrP antibody (100 nM for 20 min), which was shown to block Aβ42 binding acutely (Fig. 3). Pretreatment with control immunoglobulin G did not reduce the suppression of LTP by Aβ42 oligomer (Fig. 4d). In contrast, the 6D11-pretreated wild-type slices were protected from LTP suppression by the later addition of Aβ42-oligomer preparations (Fig. 4d). Thus, we conclude that PrP^C exerts a receptor action acutely to mediate Aβ42-oligomer inhibition of synaptic plasticity in the hippocampal slice.

The principal finding of this study is that PrP^C functions as a receptor to mediate the deleterious effects of the Aβ42 oligomer. This hypothesis is supported by our isolation of PrP^C as an Aβ42-oligomer-binding site in an unbiased genome-wide screen, by the match between PrP^C expression and the properties of Aβ42-oligomer-binding sites, and by the localization of amyloid-β binding to a neurodegeneration-associated domain of PrP^C. Although PrP^C is not the sole binding site for amyloid-β oligomers on hippocampal neurons, it is essential for Aβ42-oligomer inhibition of hippocampal LTP. Several publications indirectly support coupling of Aβ42 oligomers and PrP^C. For example,

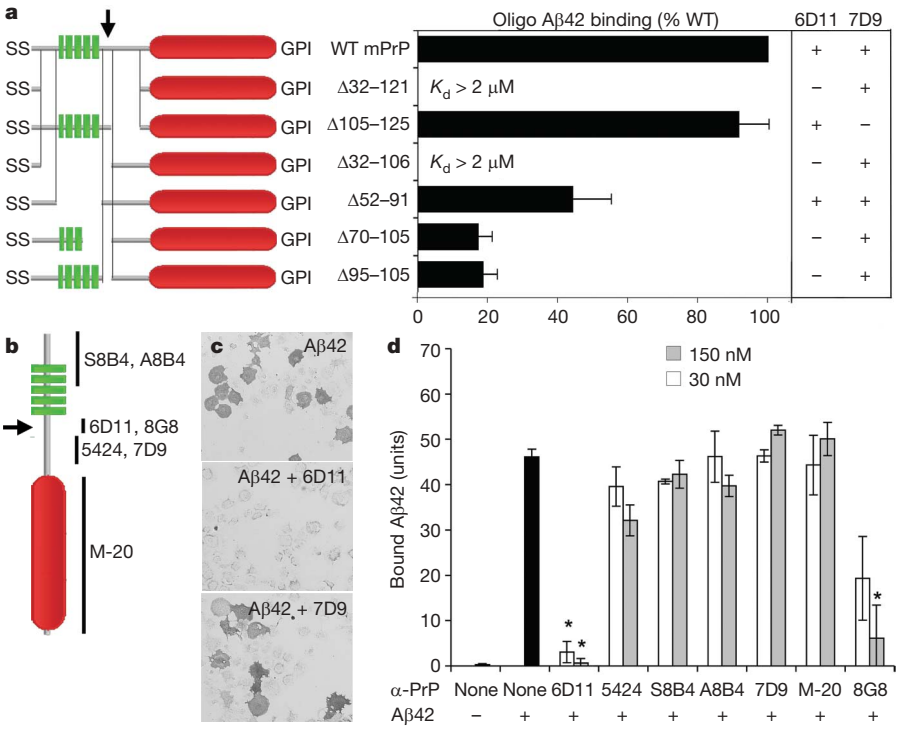

Figure 3 | Aβ42 oligomers bind to residues 95–110 of PrP^C. **a**, COS-7 cells were transfected with expression plasmids directing the expression of each of the indicated PrP deletion mutants (green, octapeptide repeats; red, globular domain; SS, signal sequence). Transfected cells were assessed for binding of oligomeric Aβ42, or by live cell immunocytochemistry with 6D11 and 7D9 anti-PrP antibodies. Mean and s.e.m. from four experiments. **b**, Schematic of antibody epitopes. **c**, **d**, PrP^C-expressing COS-7 cells were analysed for oligomeric Aβ42 binding after exposure to the various anti-PrP antibodies for 1 h. 6D11 and 8G8 but not other antibodies block Aβ42-oligomer binding. Data are mean ± s.e.m. from four experiments. Inhibition of binding by 6D11 or 8G8 is significant (*$P < 0.02$, analysis of variance, ANOVA).

a polymorphism in *Prnp* gene is associated with Alzheimer's disease in certain populations[24] and with long-term memory formation in the general population[25]. Amongst several proteins found in PrP^C immunoprecipitates are APP and the related proteins APLP1 and APLP2 (refs 26 and 27).

Glutamate receptors are central to LTP and their modulation has been implicated in deleterious synaptic amyloid-β action[5,8,28,29]. Recently, PrP^C has been shown to interact with *N*-methyl-D-aspartate receptor subunit 2D (NR2D, also known as GRIN2D), and to modulate its function[30]. We assessed whether Aβ42 interaction might regulate glutamate receptors directly through PrP^C. When expressed in a heterologous *Xenopus laevis* oocyte system, GluR1–4 (GRIA1–4) receptors and NR2B (GRIN2B)- and NR2D-containing receptors are insensitive to Aβ42 oligomers, with or without PrP^C co-expression (Supplementary Figs 14 and 15). This is consistent with previous observations that amyloid-β drives glutamate receptor redistribution in neurons together with morphologic changes in dendrites[5,8,9]. Thus,

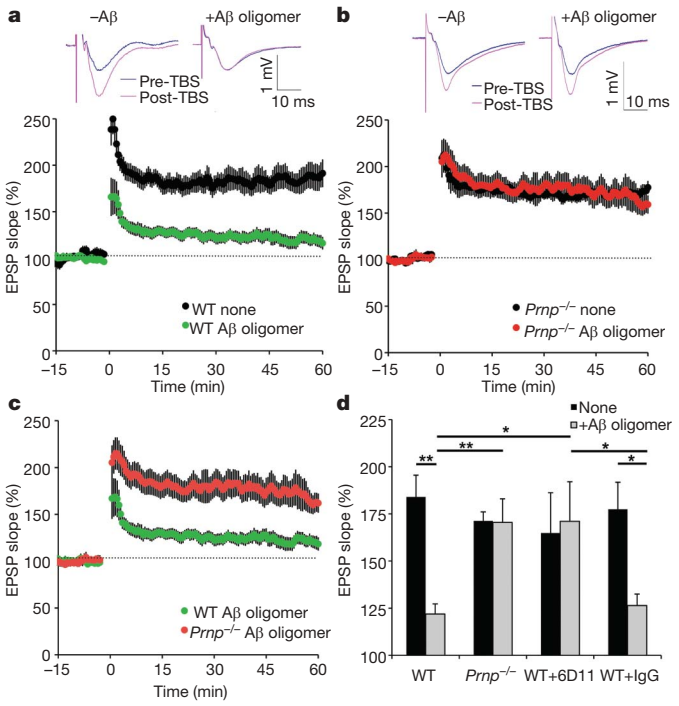

Figure 4 | PrP^C is required for Aβ42 oligomer inhibition of hippocampal LTP. **a**, Field potentials were recorded from the CA1 region of hippocampal slices from adult wild-type mice with or without the addition of 500 nM oligomeric Aβ42 to the perfusion 20–40 min before theta burst stimulation (TBS). The top panels show traces before and after TBS. The slope of the EPSP relative to the pre-TBS level is a plotted as a function of time in the lower panel. Data are mean ± s.e.m. from separate slices. For no peptide, $n = 12$ slices from 9 mice; for amyloid-β oligomer, $n = 31$ slices from 14 mice. **b**, CA1 potentials were recorded from slices of mice lacking PrP expression by the same method as in **a**. There is no significant inhibition of LTP by oligomeric Aβ42. For no peptide, $n = 10$ slices from 7 mice; for amyloid-β oligomer, $n = 35$ slices from 15 mice. **c**, The CA1 EPSP slope in wild-type and $Prnp^{-/-}$ slices was recorded in the presence of oligomeric Aβ42 by an observer blind to the genotype and is replotted from panels **a** and **b**. For the values 30–60 min post-TBS, the EPSPs were significantly greater in the $Prnp^{-/-}$ slices by repeated measures ANOVA, $P = 0.005$. For WT, $n = 31$ slices from 14 mice; for $Prnp^{-/-}$, $n = 35$ slices from 15 mice. **d**, The magnitude of LTP between 30 min and 60 min is plotted as a function of genotype, the addition of 6D11 antibody, control immunoglobulin G (IgG) and/or Aβ42 oligomer before the induction of LTP. Data are mean and s.e.m. For 6D11 without amyloid-β, $n = 7$; for 6D11 plus amyloid-β, $n = 6$. For IgG without amyloid-β, $n = 8$; for IgG plus amyloid-β, $n = 6$. The indicated comparisons are significant at **$P < 0.01$ or *$P < 0.05$, ANOVA. Untreated, IgG and 6D11 slices without Aβ42 did not differ significantly.

the Aβ42-oligomer interaction with PrP^C is likely to initiate a signalling cascade that is not operative in oocytes, but one that is capable of modifying synaptic morphology and function in the brain. The mechanism by which Aβ42-oligomer binding to PrP^C participates in Alzheimer's disease appears unrelated to the infectious PrP^{Sc} conformation of PrP. In this regard, the neurodegeneration reported in transgenic mice expressing truncated forms of PrP^C may be more relevant[17,18]. A putative PrP^C-associated transmembrane co-receptor is likely to have a central role in Alzheimer's-disease-mediated neurodegeneration. PrP^C-specific reagents will provide molecular tools to dissect the cellular basis for Aβ42-oligomer-induced changes in synaptic function. The interaction between amyloid-β and PrP^C provides a new site for the development of therapeutics designed to relieve Alzheimer's disease symptoms.

METHODS SUMMARY

Mouse strains. $Prnp^{-/-}$ mice (Edinburgh strain)[21] on an inbred C57Bl6 background were obtained from B. Chesebro and $Prnp^{-/-}$ mice (Zurich I)[20] on a mixed strain background were obtained from the European Mutant Mouse Archive.

Aβ42 preparation and cellular binding. Aβ42 oligomer preparations were generated from synthetic peptide[4]. For binding assays, COS-7 cells were transiently transfected with cDNA expression plasmids or isolated hippocampal neurons were cultured from E18 embryos. Bound biotin–Aβ42 was detected using avidin conjugates.

Electrophysiology. Hippocampal slices (400 μm) from C57Bl6J or $Prnp^{-/-}$ mice were bathed in oxygenated artificial cerebrospinal fluid. The Schaffer collateral pathway was stimulated at 0.033 Hz at levels that evoked less than 50% of maximal field EPSPs. Evoked CA1 field potentials were recorded and the slope of the EPSP determined (Clampfit, Molecular Devices). Aβ42 or antibodies were bath-applied for 20–40 min before inducing LTP with ten 100-Hz trains at five pulses delivered at 5 Hz.

Full Methods and any associated references are available in the online version of the paper at www.nature.com/nature.

Received 12 May 2008; accepted 7 January 2009.

1. Hardy, J. & Selkoe, D. J. The amyloid hypothesis of Alzheimer's disease: progress and problems on the road to therapeutics. *Science* **297,** 353–356 (2002).
2. Lesne, S. *et al.* A specific amyloid-β protein assembly in the brain impairs memory. *Nature* **440,** 352–357 (2006).
3. Cleary, J. P. *et al.* Natural oligomers of the amyloid-β protein specifically disrupt cognitive function. *Nature Neurosci.* **8,** 79–84 (2005).
4. Chromy, B. A. *et al.* Self-assembly of $Aβ_{1-42}$ into globular neurotoxins. *Biochemistry* **42,** 12749–12760 (2003).
5. Lacor, P. N. *et al.* Abeta oligomer-induced aberrations in synapse composition, shape, and density provide a molecular basis for loss of connectivity in Alzheimer's disease. *J. Neurosci.* **27,** 796–807 (2007).
6. Lacor, P. N. *et al.* Synaptic targeting by Alzheimer's-related amyloid β oligomers. *J. Neurosci.* **24,** 10191–10200 (2004).
7. Walsh, D. M. *et al.* Naturally secreted oligomers of amyloid β protein potently inhibit hippocampal long-term potentiation *in vivo*. *Nature* **416,** 535–539 (2002).
8. Shankar, G. M. *et al.* Natural oligomers of the Alzheimer amyloid-β protein induce reversible synapse loss by modulating an NMDA-type glutamate receptor-dependent signaling pathway. *J. Neurosci.* **27,** 2866–2875 (2007).
9. Shankar, G. M. *et al.* Amyloid-β protein dimers isolated directly from Alzheimer's brains impair synaptic plasticity and memory. *Nature Med.* **14,** 837–842 (2008).
10. Hepler, R. W. *et al.* Solution state characterization of amyloid β-derived diffusible ligands. *Biochemistry* **45,** 15157–15167 (2006).
11. Lambert, M. P. *et al.* Diffusible, nonfibrillar ligands derived from $Aβ_{1-42}$ are potent central nervous system neurotoxins. *Proc. Natl Acad. Sci. USA* **95,** 6448–6453 (1998).
12. Prusiner, S. B. Prions. *Proc. Natl Acad. Sci. USA* **95,** 13363–13383 (1998).
13. Yan, S. D. *et al.* RAGE and amyloid-β peptide neurotoxicity in Alzheimer's disease. *Nature* **382,** 685–691 (1996).
14. Wang, H. Y. *et al.* β-$Amyloid_{1-42}$ binds to α7 nicotinic acetylcholine receptor with high affinity. Implications for Alzheimer's disease pathology. *J. Biol. Chem.* **275,** 5626–5632 (2000).
15. Viles, J. H. *et al.* Copper binding to the prion protein: structural implications of four identical cooperative binding sites. *Proc. Natl Acad. Sci. USA* **96,** 2042–2047 (1999).
16. Jackson, G. S. *et al.* Location and properties of metal-binding sites on the human prion protein. *Proc. Natl Acad. Sci. USA* **98,** 8531–8535 (2001).
17. Baumann, F. *et al.* Lethal recessive myelin toxicity of prion protein lacking its central domain. *EMBO J.* **26,** 538–547 (2007).
18. Li, A. *et al.* Neonatal lethality in transgenic mice expressing prion protein with a deletion of residues 105–125. *EMBO J.* **26,** 548–558 (2007).
19. Riek, R. *et al.* NMR structure of the mouse prion protein domain PrP(121–321). *Nature* **382,** 180–182 (1996).
20. Bueler, H. *et al.* Normal development and behaviour of mice lacking the neuronal cell-surface PrP protein. *Nature* **356,** 577–582 (1992).
21. Manson, J. C. *et al.* 129/Ola mice carrying a null mutation in PrP that abolishes mRNA production are developmentally normal. *Mol. Neurobiol.* **8,** 121–127 (1994).
22. Lledo, P. M., Tremblay, P., DeArmond, S. J., Prusiner, S. B. & Nicoll, R. A. Mice deficient for prion protein exhibit normal neuronal excitability and synaptic transmission in the hippocampus. *Proc. Natl Acad. Sci. USA* **93,** 2403–2407 (1996).
23. Curtis, J., Errington, M., Bliss, T., Voss, K. & MacLeod, N. Age-dependent loss of PTP and LTP in the hippocampus of PrP-null mice. *Neurobiol. Dis.* **13,** 55–62 (2003).
24. Riemenschneider, M. *et al.* Prion protein codon 129 polymorphism and risk of Alzheimer disease. *Neurology* **63,** 364–366 (2004).
25. Papassotiropoulos, A. *et al.* The prion gene is associated with human long-term memory. *Hum. Mol. Genet.* **14,** 2241–2246 (2005).
26. Yehiely, F. *et al.* Identification of candidate proteins binding to prion protein. *Neurobiol. Dis.* **3,** 339–355 (1997).
27. Schmitt-Ulms, G. *et al.* Time-controlled transcardiac perfusion cross-linking for the study of protein interactions in complex tissues. *Nature Biotechnol.* **22,** 724–731 (2004).
28. Venkitaramani, D. V. *et al.* β-amyloid modulation of synaptic transmission and plasticity. *J. Neurosci.* **27,** 11832–11837 (2007).
29. Hsieh, H. *et al.* AMPAR removal underlies Aβ-induced synaptic depression and dendritic spine loss. *Neuron* **52,** 831–843 (2006).
30. Khosravani, H. *et al.* Prion protein attenuates excitotoxicity by inhibiting NMDA receptors. *J. Cell Biol.* **181,** 551–565 (2008).

Supplementary Information is linked to the online version of the paper at www.nature.com/nature.

Acknowledgements We thank S. Tomita for cRNAs encoding GluR1–4 and stargazin (also known as CACNG2), B. Chesebro for providing us the *Prnp* null mice, M. Schachner for providing the PrP–Fc expression vector, E. Flechsig, C. Weismann and D. Harris for providing the PrP^C deletion expression plasmids, D. Westaway for the Sprn expression plasmid and P. Seeburg for *N*-methyl-D-aspartate receptor subunit cDNAs. We thank S. Sodi for assistance with mouse husbandry. We thank E. Folta-Stogniew for SEC, and C. Rahner and M. Graham for electron microscopy. J.L. is a Brown-Coxe Postdoctoral Fellow, J.W.G. is supported by NIH Medical Scientist training Program grant 5T32GN07205, and S.M.S. is a member of the Kavli Institute for Neuroscience at Yale University. This work was supported by research grants from the Falk Medical Research Trust and the NIH to S.M.S. The SEC was supported by a NIDA-funded Neuroproteomic Center.

Author Contributions J.L. performed the amyloid-β binding and expression cloning experiments, D.A.G. conducted mouse breeding and tissue biochemistry, S.M.S. and H.B.N. performed the hippocampal electrophysiology experiments, and S.M.S., J.W.G. and J.L. performed the *X. laevis* studies. S.M.S. supervised all experiments. All authors participated in writing the manuscript.

Author Information Reprints and permissions information is available at www.nature.com/reprints. Correspondence and requests for materials should be addressed to S.M.S. (stephen.strittmatter@yale.edu).

METHODS

Aβ42 preparations. Oligomerized human Aβ42 was prepared as described[5,6] with minor modifications. Aβ42 peptide or Aβ42 with a biotin moiety attached by 6-carbon linker to the N terminus (both synthesized at Yale in the Keck Biotechnology Resource Laboratory, ~99% pure) were dissolved in 1,1,1,3,3,3-hexafluoro-2-propanol, dried and stored at −80 °C. The dried peptide was reconstituted in anhydrous DMSO at 100 mM, and then diluted in F12 media (Invitrogen) to a final concentration of 100 μM. After 16 h incubation at 22 °C, the preparation was centrifuged at 21,000*g* for 15 min, and the supernatant was collected for experiments.

Mouse strains. *Prnp*$^{-/-}$ mice (Edinburgh strain)[21] on an inbred C57Bl6 background (greater than ten backcrosses) were obtained from B. Chesebro, and *Prnp*$^{-/-}$ mice (Zurich I)[20] on a mixed strain background were obtained from the European Mutant Mouse Archive. All electrophysiological strain comparisons were completed by experimentalists unaware of the mouse genotype.

Biophysical characterization of Aβ42 oligomers. For electron microscopic analysis, oligomerized human Aβ42 was prepared as above. Fresh Aβ42 was prepared by dissolving dried peptide similarly into DMSO and then into F12 media immediately before use. Aβ42 fibrils were prepared by dissolving dried peptide in DMSO and then diluting into PBS followed by 24 h incubation at 37 °C with 100 r.p.m. mixing. All Aβ42 preparations were stained with 2% phosphotungstic acid (pH 7.0) for 2 min and imaged with Tecnai 12 Biotwin transmission electron microscope at 160,000-fold magnification. For analysis of the molecular weight of oligomerized human Aβ42, SEC combined with light scattering analysis was used. The SEC data were collected using a sequential connection of Superdex 200, Superdex 75, and Superdex peptide, 10/30, HR SEC columns (GE Healthcare), connected to high-performance liquid chromatography system, Alliance 2965 (Waters Corp.), equipped with an autosampler. The elution from SEC was monitored by a photodiode array (PDA) UV/VIS detector (996 PDA, Waters Corp.), differential refractometer (OPTI-rEx, Wyatt Corp.) and static, multiangle laser LS detector (DAWN-EOS, Wyatt Corp.). The SEC-UV/LS/RI system was equilibrated in F12 media at the flow rate of 0.5 ml min^{-1}. Two software packages were used for data collection and analysis: the Millennium software (Waters Corp.) controlled the high-performance liquid chromatography operation and data collection from the multi-wavelength UV/VIS detector, whereas the ASTRA software (Wyatt Corp.) collected data from the light scattering detector, and recorded the UV trace at 220 nm sent from the PDA detector. The weight average molecular masses were determined across the entire elution profile in the intervals of 1 s from the static LS measurement using the ASTRA software as described previously[31].

Expression cloning and COS-7 cell binding assays. We screened an arrayed adult mouse brain cDNA library (Origene) of 225,000 clones by transfecting COS-7 cells with pools of 5,000 clones, and visually inspecting for those rare cells transfected with a cDNA conferring Aβ42-oligomer binding. Two days after transfection, the cells were incubated with Aβ42 oligomers (1 μM total Aβ42 monomer concentration) in F12 media at 22 °C for 2 h. Next, unbound Aβ42 was removed by extensive washing with F12 media. The cells were fixed with 3.7% formaldehyde, washed three times with PBS, incubated in 65 °C for 2 h, blocked for 20 min with 3% goat serum and 0.1% Triton X-100 in PBS, and incubated for 16 h with alkaline-phosphatase-conjugated steptavidin in PBS supplemented with 1.5% goat serum and 0.05% Triton X-100. Finally, bound alkaline phosphatase was visualized by 5-bromo-4-chloro-3-indolyl phosphate/nitro blue tetrazolium reaction. The initial screen was followed by sequential fractionation of sub-pools. This process led to identification of two independent cDNA clones mediating high-affinity binding of Aβ42 oligomers to transfected COS-7 cells. Sequencing of the inserts revealed that both clones encode full-length PrP^{C}. We also performed a directed experiment to identify putative low-affinity Aβ42-oligomer receptor(s): a library consisting of 352 individual preparations of cDNAs encoding transmembrane proteins (GFC-transfection array panel, Origene) was transfected into COS-7 cells, and binding was detected as above. We also tested similarly several candidate receptors; the cDNA plasmids were obtained from Origene or Open Biosystems. Quantification of bound Aβ42 to PrP-transfected COS-7 cells was performed with ImageJ similarly to that described previously[32–35].

For analysis of oligomeric Aβ42 binding to mouse PrP deletion constructs, the indicated constructs were transfected into COS-7 cells. PrP Δ105–125 expression construct was provided by D. Harris[18]. PrP Δ32–121, PrP Δ32–106 and PrP Δ52–91 were provided by E. Flechsig and C. Weismann[36]. To obtain PrP Δ70–105 and PrP Δ95–105 expression constructs, nucleotides encoding mouse PrP amino acids 106–254 and the C-terminal stop codon were PCR-amplified with primers containing EcoRI and XhoI sites, and the fragment was cloned into EcoRI and XhoI sites of pcDNA3.1/mycHis A (Invitrogen). Next, nucleotides encoding mouse PrP amino acids 1–69 or 1–94 were PCR-amplified with primers containing HindIII and EcoRI sites, and the fragments were cloned into HindIII and EcoRI sites of the above-mentioned PrP 106–254 pcDNA3.1/mycHis A construct.

For double-immunostaining of PrP^{C} expressed on COS-7 cells and bound non-biotinylated Aβ42, the rabbit anti-Aβ42 antibody (Cell Signaling Technology) was used in combination with 7D9 PrP mouse monoclonal antibody (Covance). Alexa Fluor 488 goat anti-rabbit and 568 goat anti-mouse secondary antibodies (Invitrogen) were used. No specific signal was obtained with amyloid-β antibody without the addition of amyloid-β on PrP-expressing cells, or when incubating amyloid-β with non-transfected control cells.

Antibody blocking experiments. The following PrP antibodies were used: S8B4 (mouse monoclonal; epitope mapped to amino acids 32–69 of PrP (Supplementary Fig. 8), 8B4 clone from Santa Cruz Biotechnology), M-20 (affinity-purified goat polyclonal; raised against peptide located in the C-terminal half of mouse PrP (Supplementary Fig. 8), Santa Cruz Biotechnology), 7D9 (mouse monoclonal; according to manufacturer epitope between amino acids 105 and 125 of mouse PrP, Covance/Signet), 6D11 (mouse monoclonal; according to manufacturer epitope between amino acids 93 and 109, Covance/Signet), A8B4 (mouse monoclonal; according to manufacturer epitope between amino acids 37 and 44 of mouse PrP, 8B4 clone from Alicon GH), MAB5424 (mouse monoclonal; epitope mapped to amino acids 105–125 (Supplementary Fig. 8), Chemicon), and 8G8 (mouse monoclonal; epitope between amino acids 95 and 110, Cayman Chemical/SPIbio). In live-cell staining application, all antibodies robustly recognized PrP expressed on COS-7 cells (Supplementary Fig. 8). To detect the blockade of Aβ42–PrP interaction, COS-7 cells transfected 2 days earlier with PrP expression vector were pre-incubated with the indicated concentrations of antibodies in F12 media at 22 °C for 1 h. Next, biotin–Aβ42 oligomers were added to a final concentration of 250 nM for 2 h. Finally, bound Aβ42 was visualized as described previously.

PrP–Fc pull-down experiments. HEK293T cells were transiently transfected with expression vector encoding mouse PrP (codon 1–230, devoid of GPI-anchor modification sequence) fused to the Fc region of human IgG1 (ref. 37). Secreted PrP–Fc fusion was bound on protein G Sepharose CL-4B (GE Healthcare), and contaminants were removed by washes with increasing concentrations of buffered NaCl solution. Control human IgG Fc fragment (Bethyl Laboratories) was similarly coupled to protein G Sepharose. Aged oligomerized or fresh Aβ42 was incubated with Fc proteins for 2 h at 4 °C, washed extensively with F12, and the bound material was analysed by western blotting with 6E10 amyloid-β antibody. For quantification of bound material, infrared fluorescence secondary antibodies were used in combination with Odyssey infrared imaging system (LI-COR Biosciences); the signal across the whole lane was quantified with Odyssey software. The reported result is average ± s.e.m. from four experiments.

Neuron cultures and neuronal binding assays. Rat and mouse E18 hippocampal neurons were cultured in Neurobasal-A media supplemented with B-27, 0.5 mM L-glutamine, penicillin and streptomycin (all from Invitrogen) on tissue culture plates or on Lab-Tek II-CC2 chamber slides (Nunc) coated with poly-L-lysine and laminin. For the analysis of PrP expression, neurons were lysed with RIPA buffer after the indicated time *in vitro*. Also wild-type and *Prnp*$^{-/-}$ mouse brain lysates and PrP-expressing HEK293T cell lysates were prepared. The lysates were analysed by western blotting with 8H4 anti-PrP antibody (Alicon AG), anti-βIII-tubulin antibody (Covance), and anti-GAPDH antibody (Sigma). To remove carbohydrate-moieties from PrP, some samples were treated with PNGase F (New England Biolabs). For immunocytochemistry, the following antibodies were used: anti-PrP (mouse monoclonal, 8H4 clone, Alicon AG), anti-MAP2 (chicken polyclonal, Chemicon) and anti-PSD95 (rabbit polyclonal, Zymed/Invitrogen). For rat neurons, binding of Aβ42 was determined as in COS-7 cell binding assays. To determine bound biotin Aβ42 oligomers in wild-type and *Prnp*$^{-/-}$ cultures, an Aβ42-oligomer concentration equivalent to 80 nM of monomer Aβ42 (~0.3 nM oligomer) was used. The bound biotin–Aβ42-oligomers were visualized with NeutrAvidin Oregon Green 488 conjugate (Invitrogen) and dendrites with anti-MAP2 antibody (chicken polyclonal, Chemicon). Fluorescent images were captured at ×63 with fixed illumination and exposures, and then processed using NIH Image. Integrated signal intensity for bound Aβ42 oligomer in puncta of less than 50 μm^2 was measured after thresholding and background subtraction across both wild-type and *Prnp*$^{-/-}$ images. The integrated punctate amyloid-β signal was divided be the area of MAP-2-positive dendrite in each image, to generate units of Aβ42 oligomer binding to puncta per dendritic area.

Electrophysiology. Adult (2–6 months of age) C57BL/6J or *Prnp*$^{-/-}$ mice were decapitated, and their brains rapidly removed and immersed in ice-cold artificial cerebrospinal fluid (aCSF). The composition of the aCSF was as follows: 119 mM NaCl, 2.5 mM KCl, 1.3 mM $MgCl_2$, 2.4 mM $CaCl_2$-, 26.2 mM $NaHCO_3$, 11 mM D-glucose, 1.25 mM NaH_2PO_4. Coronal sections (400 μm) were prepared on a Vibratome 1000 Plus, using stainless steel razor blades. Slices were allowed to recover for at least 2 h in a submerged incubation chamber (BSC-PC, Warner

Instruments) at room temperature, continuously bubbled with a mixture of 95% O_2 and 5% CO_2.

For extracellular recordings, slices were submerged in a recording chamber (RC-27L, Warner Instruments), continuously perfused with oxygenated aCSF at a rate of 2 ml min^{-1} at 30 °C. A bipolar tungsten microelectrode (TM33CCNON, World Precision Instruments) was used to stimulate Schaffer collateral fibres, and extracellular field EPSPs were recorded using a glass microelectrode (2–6 MΩ) filled with aCSF in the stratum radiatum of CA1. For all experiments, test stimuli were given at 0.033 Hz, and the stimulus intensity was set to give baseline field EPSP slopes of less than 50% of the maximal response. A stable baseline was recorded for at least 20 min before inducing LTP. LTP was induced by theta burst stimulation (10 bursts of 4 shocks at 100 Hz, with an interburst interval of 200 ms) given at baseline intensity. Field potentials were recorded using an Axon Intruments 700B amplifier and a Digidata 1440A digitizer, and data were analysed using pClamp 10 software (Molecular Devices).

Experiments with $Prnp^{-/-}$ mice were conducted in a blinded fashion with respect to genotype. Aβ42 oligomers (500 nM), 6D11 anti-PrP^C antibody (5 μg ml^{-1}) and mouse IgG (Sigma-Aldrich, 5 μg ml^{-1}) were diluted in aCSF. For experiments using amyloid-β, prion protein antibody or IgG alone, submerged slices were continually perfused with aCSF containing one of these for 20–40 min before LTP induction, and the same aCSF was recycled for the duration of the recording. For experiments using a combination of amyloid-β oligomers with either anti-PrP antibody or IgG, slices were first perfused with aCSF containing antibody or IgG for 20–40 min followed by the addition of aCSF containing amyloid-β oligomers, and perfused for at least another 20 min before LTP induction. The aCSF was recycled, ensuring the presence of amyloid-β oligomers with either antibody or IgG for the duration of the recording.

Similar results were obtained with the Zurich I and the Edinburgh $Prnp^{-/-}$ mice (Supplementary Fig. 13), and the pooled results are presented in Fig. 4.

31. Folta-Stogniew, E. Oligomeric states of proteins determined by size-exclusion chromatography coupled with light scattering, absorbance, and refractive index detectors. *Methods Mol. Biol.* **328,** 97–112 (2006).
32. Rajagopalan, S. *et al.* Neogenin mediates the action of repulsive guidance molecule. *Nature Cell Biol.* **6,** 756–762 (2004).
33. Fournier, A. E., GrandPre, T. & Strittmatter, S. M. Identification of a receptor mediating Nogo-66 inhibition of axonal regeneration. *Nature* **409,** 341–346 (2001).
34. Takahashi, T. *et al.* Plexin–neuropilin-1 complexes form functional semaphorin-3A receptors. *Cell* **99,** 59–69 (1999).
35. Takahashi, T., Nakamura, F., Jin, Z., Kalb, R. G. & Strittmatter, S. M. Semaphorins A and E act as antagonists of neuropilin-1 and agonists of neuropilin-2 receptors. *Nature Neurosci.* **1,** 487–493 (1998).
36. Weissmann, C. & Flechsig, E. PrP knock-out and PrP transgenic mice in prion research. *Br. Med. Bull.* **66,** 43–60 (2003).
37. Chen, S., Mange, A., Dong, L., Lehmann, S. & Schachner, M. Prion protein as trans-interacting partner for neurons is involved in neurite outgrowth and neuronal survival. *Mol. Cell. Neurosci.* **22,** 227–233 (2003).